Journal of Controlled Release 371 (2024) 179–192

Contents lists available at ScienceDirect

Journal of Controlled Release

journal homepage: www.elsevier.com/locate/jconrel

Mucoadhesive film for oral delivery of vaccines for protection of the respiratory tract

Hana Esih [a,b,1], Klemen Mezgec [a,b,1], Martina Billmeier [c], Špela Malenšek [a,b], Mojca Benčina [a,d], Blaž Grilc [e], Sara Vidmar [a,b], Mirjana Gašperlin [e], Marjan Bele [f], Mihaela Zidarn [g], Tatjana Lejko Zupanc [h], Tina Morgan [g], Ingo Jordan [i], Volker Sandig [i], Silke Schrödel [j], Christian Thirion [j], Ulrike Protzer [k], Ralf Wagner [c,l], Duško Lainšček [a,d,*], Roman Jerala [a,d,*]

[a] Department of Synthetic Biology and Immunology, National Institute of Chemistry, 1000 Ljubljana, Slovenia
[b] Graduate School of Biomedicine, University of Ljubljana, 1000 Ljubljana, Slovenia
[c] Institute of Medical Microbiology & Hygiene, Molecular Microbiology (Virology), University of Regensburg, Regensburg, Germany
[d] Centre for Technologies of Gene and Cell Therapy, 1000 Ljubljana, Slovenia
[e] University of Ljubljana, Faculty of Pharmacy, Department of Pharmaceutical Technology, Ljubljana 1000, Slovenia
[f] Department of Materials Chemistry, National Institute of Chemistry, Ljubljana 1000, Slovenia
[g] University Clinic of Pulmonary and Allergic Diseases Golnik, Golnik, Slovenia
[h] University Medical Center Ljubljana, 1000 Ljubljana, Slovenia
[i] Applied Science & Technologies, ProBioGen AG, Berlin, Germany
[j] SIRION Biotech GmbH, Am Klopferspitz 19, 82152 Martinsried, Germany
[k] Institute of Virology, School of Medicine, Technical University of Munich, Helmholtz Zentrum München, Munich, Germany
[l] Institute of Clinical Microbiology & Hygiene, University Hospital, Regensburg, Germany

ARTICLE INFO

Keywords:
Vaccine delivery
Mucoadhesive film
Mucosal immunity
Respiratory infection

ABSTRACT

The delivery of vaccines plays a pivotal role in influencing the strength and longevity of the immune response and controlling reactogenicity. Mucosal immunization, as compared to parenteral vaccination, could offer greater protection against respiratory infections while being less invasive. While oral vaccination has been presumed less effective and believed to target mainly the gastrointestinal tract, trans-buccal delivery using mucoadhesive films (MAF) may allow targeted delivery to the mucosa. Here we present an effective strategy for mucosal delivery of several vaccine platforms incorporated in MAF, including DNA plasmids, viral vectors, and lipid nanoparticles incorporating *mRNA* (mRNA/LNP). The mRNA/LNP vaccine formulation targeting SARS-CoV-2 as a proof of concept remained stable within MAF consisting of slowly releasing water-soluble polymers and an impermeable backing layer, facilitating enhanced penetration into the oral mucosa. This formulation elicited antibody and cellular responses comparable to the intramuscular injection, but also induced the production of mucosal IgAs, highlighting its efficacy, particularly for use as a booster vaccine and the potential advantage for protection against respiratory infections. The MAF vaccine preparation demonstrates significant advantages, such as efficient delivery, stability, and simple noninvasive administration with the potential to alleviate vaccine hesitancy.

1. Introduction

Vaccination is a highly efficacious method to prevent the spread and limit the pathology of highly contagious and debilitating diseases. Remarkable advancements have been made in the field of vaccinology, particularly in the areas of antigen design and the mRNA/LNP platform. Nevertheless, a need for novel immunization strategies remains, particularly in addressing psychological factors such as vaccine hesitancy and trypanophobia (the fear of needles), vaccine inequity caused by supply limitations, and immunological challenges that include induction of persistent immune responses and robust mucosal immunity [1,2]. Particularly in the context of respiratory diseases such as COVID-

* Corresponding authors at: Department of Synthetic Biology and Immunology, National Institute of Chemistry, 1000 Ljubljana, Slovenia.
E-mail addresses: dusko.lainscek@ki.si (D. Lainšček), roman.jerala@ki.si (R. Jerala).
[1] These two authors contributed equally

https://doi.org/10.1016/j.jconrel.2024.05.041
Received 5 February 2024; Received in revised form 20 May 2024; Accepted 21 May 2024
Available online 29 May 2024

19, it is desirable to achieve stronger mucosal immunity compared to what can be achieved by the systemic immune responses after administering vaccines by intramuscular injection (IM) [3]. Implementation of non-invasive mucosal vaccines is expected to improve patient compliance (especially in those with trypanophobia, the fear of needles) and provide more effective and longer-lasting protection against respiratory, sexually transmitted, and gastrointestinal infections, where the mucosal surfaces serve as the primary entry site for pathogens [4,5].

Mucosal vaccination mimics natural infection by eliciting both innate and adaptive immune responses through the mucosa-associated lymphoid tissues. Currently, there are only a few mucosal vaccines approved for human use, mostly based on live attenuated or inactivated pathogens. Approved mucosal vaccines include intranasal vaccine against influenza and oral vaccines for typhoid, cholera, rotavirus and poliomyelitis [6,7]. Intranasal delivery (IN) presents an appealing route for vaccine administration, offering advantages such as ease of self-administration and stimulation of mucosal immunity [8]. However, the specific physiological features of the nasal cavity can hinder the attachment of antigens to the epithelium [9,10]. On the other hand, oral vaccines are administered into the gut, targeting the gut-associated lymphoid tissue, which is an essential site for eliciting immune responses. Gut-associated lymphoid tissue consists of organized lymphoid tissues, such as mesenteric lymph nodes and Peyer's patches, specialized lymphoid follicles, which play a critical role in initiating specific antigen immune responses. However, associated challenges include low efficiency of delivery into the lymph nodes proximal to the respiratory tract with low protection against respiratory pathogens, interference with the normal gut microbiota and gastrointestinal degradation with low bioavailability due to the instability and inability to pass through gastrointestinal barriers [11]. An alternative mode of oral delivery through the buccal mucosa could ameliorate this issue, as it would bypass the digestive tract and provide a slow-release profile to the mucosa towards the immune cells in head lymph nodes and at the same time avoid any potential risk of delivery to the brain. Transbuccal delivery could be achieved by the application of a mucoadhesive film (MAF), which adheres to the buccal mucosa and releases the active agents in a controlled manner, providing easy-to-apply targeted delivery and preventing loss to the gut. The design of a buccal film in most cases includes multiple layers. The outermost layer forms the backing layer, which is usually made of an impermeable material. Its main function is to act as a protective barrier, provide structural support and facilitate unidirectional release. The active ingredient is typically formulated in the second layer, dispersed or encapsulated within a polymer matrix. For optimal penetration, the patch should be positioned in the buccal region, as it offers better permeability of non-keratinized tissue, which is more permeable than the keratinized regions like the mucosa of the hard palate. The oral mucosa has a rich blood supply and shows short recovery times after stress and is suitable for the administration of retentive dosage forms and provides direct access to the systemic circulation through the internal jugular vein. Up to now, buccal formulations have been successfully approved for clinical use for varied indications such as sedation, insomnia, angina, pain, and smoking cessation [12]. Other buccal liposomal formulations that have been previously described include silymarin liposomes [13], buccal micellar spray, and buccal deformable liposomes to deliver insulin [14]. There has been significant progress in delivering viral particles and nanoparticles capable of penetrating the buccal mucosa, with sizes of up to 200 nm. Moreover, advancements in buccal film manufacturing, with technologies like 2D and 3D printing (inkjet printing), electrospraying, electrospinning, and delivery based on electroporation or iontophoresis offer potential for further development [15]. Numerous platforms draw inspiration from distinctive biological structures found in nature, such as extruded octopus- [16] or mussel-inspired films for adhesion to wet biological membranes [17]. These techniques enable control over the composition and structure of buccal films, optimizing their performance for vaccine delivery. The buccal mucosa holds great potential for vaccination due to its accessibility and the abundance of antigen-presenting cells, particularly dendritic cells, which are essential for initiating innate and adaptive immune responses. Among the recently explored strategies are MucoJet, gene guns, electrospun nanofibrous films, and microneedle-based patches. These platforms frequently induce temporary changes in the epithelium, such as microchannels, or employ electrical currents to disrupt cell membranes. They may also utilize high-voltage electrical fields to create nanopores in cell membranes, aiming to enhance the uptake of vaccine molecules by mucosal tissues [18,19]. In contrast, mucoadhesive films offer non-invasive application, which can lead to better patient acceptance and compliance, as they may be more willing to use a drug delivery system that does not involve needles or is associated with discomfort. Application of MAF can be straightforward without specialized training.

Through a rich supply of blood and lymphatic vessels, antigens from mucosal vaccines could reach antigen-presenting cells (APCs), which are abundantly present in the mucosa-associated lymphoid tissue and are responsible for antigen uptake and presentation. Activated T and B-lymphocytes are induced to migrate to *lamina propria* and glands to produce specific immune responses at the mucosal effector site, which prime the oral mucous membranes against the potential pathogen entry and reduce the risk of infection upon further exposure [20]. This approach can be particularly useful for respiratory viruses like SARS-CoV-2, which persist in the upper respiratory tract and exhibit prolonged shedding [21]. By application of mucosal vaccines, oral surfaces could be protected by secretory IgAs, in contrast to the IM route, which induces an immune response in the axillary draining lymph node that is biased towards a class switch to IgG rather than IgA [22]. Secretory IgAs can neutralize respiratory viruses or impede their attachment to epithelial cells, which makes it a prime location for local immune response to prevent infection and interrupt further transmission [23].

Given the lower effectiveness of parenteral vaccines in generating robust immune memory in upper respiratory surfaces, a promising approach to sustain and enhance the immune response could be the administration of booster doses using a mucosal-based vaccination strategy after initial intramuscular priming [24]. This method has the potential to effectively promote stronger and longer-lasting immune response and local immunity via IgA production. Several studies have already demonstrated the enhanced immunogenicity of a heterologous prime-boost regimen compared to a homologous approach [3,25]. Combining different routes of vaccine delivery could even strengthen the immune response by inducing cross-protection, as a result of enhanced local IgA and systemic IgG response. Similarly, promising results were shown with 'prime and spike' immunization with an mRNA-based vaccine boosted through an intranasal administration of recombinant antigen [3].

This study aimed to develop and test a two-layered mucoadhesive film for targeted mucosal vaccine delivery in mice. This platform is suitable for the buccal delivery of diverse vaccination platforms, including DNA plasmids, viral vectors, and mRNA packed in LNPs (mRNA/LNP). The two-layered mucoadhesive films developed here are composed of polysaccharide polymers, disaccharides, and derivatives of cellulose. The mucoadhesive layer, applied directly onto the buccal mucosa, consists of the vaccine formulation and a polymeric matrix composed of trehalose, pullulan, and sucrose. This combination of polymers provides adhesive properties to ensure attachment to the mucosal surface and controlled release of the vaccine components. The mucoadhesive layer is protected from the oral fluids with a protective water-insoluble backing layer, made of ethyl cellulose, which facilitates controlled release of active ingredients in a unidirectional manner. The platform aims to achieve directed delivery of active ingredients to the lymphoid tissue via buccal administration, thereby enhancing the efficacy of vaccination. We demonstrated an efficient delivery of nucleic acid-based vaccines, which have so far not been licensed for use as mucosal vaccines, and studied their delivery capabilities in mammalian cell lines and in an animal model. The evaluation of the films included in

vitro antigen release studies, electron microscopy imaging, and stability assessment. A short-term storage stability study was carried out to prove that incorporated antigens such as viral vectors and mRNA/LNPs withstand the process of film preparation and slow dissolution. Formulations including viral vectors and mRNA/LNP encoding SARS-CoV-2 Spike protein or its receptor binding domain were used as proof of principle to immunize animals. An extensive study of immune response was performed on MAFs delivering mRNA/LNP. The formulation triggered local IgA titers, as well as IgG and Spike-specific cytotoxic T-cell responses, which are crucial for improved immune protection against respiratory infections. We also investigated the potential of MAFs as a booster dose following parenteral priming to generate a more comprehensive immune response compared to a homologous vaccination. We conducted a study to compare the immune responses of the MAF vaccination route with intranasal (IN) and intramuscular (IM) administration (Fig. 1A). This involved evaluating both cellular and humoral response, followed by pseudoviral inhibition assays and in vivo assessments of protection against pseudovirus. To demonstrate the versatility and adaptability of the MAF platform, we performed experiments for the delivery of plasmid DNA. While the results are promising, further efficiency demonstration on another animal species will be needed to fully evaluate the potential of this application in humans. The results of this study demonstrate the potential advantages of MAF as a vaccine delivery system and likely also for other biological drugs. This platform holds promise for improving patient compliance and accessibility across various patient groups, including pediatric and geriatric populations, and for deployment in regions with limited medical resources.

2. Material and methods

2.1. Materials

Desalinized pullulan was purchased from Polyscience (USA). D-(+)-Trehalose dihydrate, Sucrose, Sodium taurodeoxycholate and Tween 80 were obtained from Sigma-Aldrich (St. Louis, Missouri, USA). Glycerol was purchased from Carlo Erba (Germany).

Ionisable cationic aminolipid heptatriacont-6,9,28,31-tetraene-19-yl 4-(dimethylamino) butanoate (DLin-MC3-DMA; MC3) was purchased at MedChemExpress. 1,2-diastearoyl-sn-glycero-3-phosphocholine (DSPC) and cholesterol (Chol) were purchased at Sigma. 1,2-dimyristoyl-glycero-3-methoxypolyethylene glycol-2000 (DMG-PEG2000) was purchased at Avanti lipids.

2.2. Methods

2.2.1. Preparation of mucoadhesive films

The backing layer consists of a mixture of 0.5 g of ethyl cellulose (30–70 mPa.s) and 0.1 g of dibutyl phthalate per 10 ml of a mixture of acetone and 2-propanol (2:1). The mixture was stirred at 200 rpm for 2 h on room temperature. The ethyl cellulose mixture was poured onto a glass film application table (ultra-flat TQC Glass Film Application Table) using a film applicator (Proceq Zua 2000). The wet mixture of the backing layer was set to a thickness of 1500 μm and left to dry overnight at ambient temperature (16 h, RT). The mucoadhesive layer was prepared from 15% *w/v* pullulan, 3,2% w/v D-(+)-Trehalose dihydrate, 3,2% w/v sucrose, and 17% of the total dry mass of glycerol dissolved in PBS and diluted to the final volume of 1 ml to form a blank film [26]. The incorporation of additives, such as plasticizers and penetration enhancers, can further improve the physical properties and enhance the penetration of incorporated antigens [27,28]. All components are

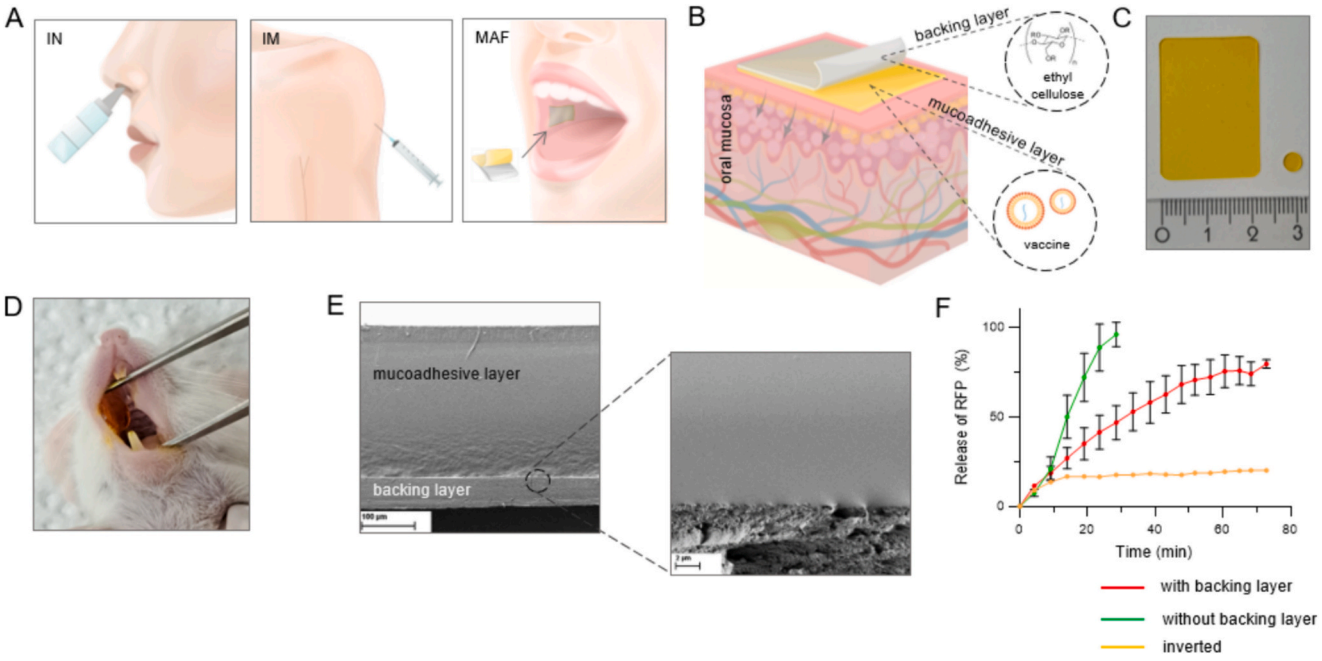

Fig. 1. Principle and properties of mucoadhesive films (MAF) for the delivery of nucleic acid-based vaccines. (**A**) Illustration of different routes of vaccine delivery: intranasal (IN), intramuscular (IM), and buccal delivery via mucoadhesive film (MAF); (**B**) Schematic representation of a bilayer mucoadhesive film attached to the oral mucosa. MAF is composed of a mucoadhesive layer (yellow) and an ethyl cellulose-based backing layer (grey), which faces the mouth cavity; (**C**) An individual film, designed for human use, which fits within the central area of the buccal mucosa, measuring 2 × 3 cm (left), alongside a smaller MAF with a 4 mm diameter used for animals (right); (**D**) MAF application to the murine buccal mucosa; (**E**) SEM micrographs of a bilayer MAF, showing the film's cross-section (left) and an interface between a mucoadhesive layer and a backing layer showing no visible separation (right); zone mag = 400×; (**F**) In vitro assessment of dissolution profiles of red fluorescent protein release from a bilayer MAF (red), MAF without a backing layer (green) and a bilayer MAF in inverted orientation (orange), using a dissolution device. The average and SD of three films are indicated for films with and without backing layer. (For interpretation of the references to colour in this figure legend, the reader is referred to the web version of this article.)

biocompatible and non-toxic, and have already been used in pharmaceutical formulations and approved for use in humans. Selected polymers are hydrophillic, which allows them to readily absorb water and form hydrated matrices. Pullulan and trehalose offer good stability, both in terms of chemical stability and physical integrity. They are resistant to enzymatic degradation in the mucosal environment, maintain the structural integrity of the film during storage and administration and are compatible with a wide range of active pharmaceutical ingredients, including hydrophilic and hydrophobic drugs, peptides, and proteins. They provide a stable and biocompatible matrix for drug encapsulation and release within mucoadhesive films [29]. Films containing active ingredients were prepared using the same protocol, where the active ingredient was mixed with the PBS solution and diluted to a final volume of 1 ml. For plasmid DNA delivery, 1 ml of the mixture contained 4000 μg of fLUC pDNA, resulting in a final film with a diameter of 4 mm containing 30 μg of pDNA (determined spectrophotometrically from electrophoretically pure plasmid isolate). For plasmid DNA delivery penetration enhancers were added with final concentrations of 1% *w/v* of Tween 80 (Sigma) or 3% w/v of STGC (Sigma). Penetration enhancers were only used for plasmid DNA delivery to avoid inactivation of viral and LNP vaccines. For plasmids and likely also proteins, enhancers play a crucial role in facilitating cellular uptake by increasing mucosal permeability [30,31].

For viral particle delivery, we added 50 μl of AV-GFP with a concentration of 1.2×10^9 IU/ml, resulting in a film with a 4 mm diameter containing approximately 1×10^5 IU of the virus. Similarly, for the MVA-GFP virus, we added 50 μl of MVA-GFP with a concentration of 4×10^8 IU/ml, resulting in a film with a 4 mm diameter containing 4×10^4 IU (GFP quantification by flow cytometry). For immunization studies using AV-RBDbann, 1×10^9 IU were added to the final mixture of mucoadhesive layer, diluted to 1 ml. For BNT162b mRNA embedded in lipid nanoparticles, we incorporated 180 μg per 1 ml of wet mixture with the final film containing 3 μg of mRNA (determined by QuantiFluor® RNA System). For mRNA/LNP encoding fLuc we added 300 μg of mRNA, resulting in a film with 5 μg of mRNA. For the dissolution study, 50 mg of RFP was added to the mixture, which was then diluted to a final volume of 1 ml, resulting in a film with a diameter of 2×3 cm, containing approximately 2 mg of the protein.

All components were premixed and magnetically stirred at approximately 100 rpm for 2 h or until thoroughly homogenized. The resulting solution was covered with parafilm and left in a fridge without stirring for 1 h to ensure there were no air bubbles in the solution. The solution containing mucoadhesive polymers was cast over the dried backing layer with a wet thickness set to 2500 μm and left to dry overnight at room temperature (16 h, RT). The last step in the manufacturing process was to cut the sheet into single-dose units. Size varied depending on the final application. Patches intended to be placed onto mouse mucosa were cut with biopsy punchers with 4 mm diameter (MM surgical), while patches prepared for dissolution studies had dimensions of $2 \text{ cm} \times 3$ cm in rectangular shape intended for human use. Prepared mucoadhesive films were subsequently stored in a petri dish until further use. All experiments included negative control, using films without active ingredients (Blank). Blank films were formulated from the same composition of mucoadhesive polymers dissolved in PBS. When appropriate for visualization (Fig. 1D), we used the food colouring agent, tartrazine (0,4 mg in 1 ml of the mixture).

2.2.2. SEM sample preparation

The mucoadhesive film was immersed in liquid nitrogen for 10 min until it hardened and turned brittle. Once the material had solidified, it was carefully broken in half to obtain a sharp cross-section for further analysis. Films were fixed on pin stubs by glue and stored in a desiccator. Scanning electron microscopy (SEM) was carried out using a Zeiss Supra TM 35 VP (Carl Zeiss, Oberkochen, Germany) field emission scanning electron microscope. The operating voltage was set to 1 kV.

2.2.3. CryoEM sample preparation

To facilitate CryoEM visualization, MAF and BNT162b2 mRNA/LNP vaccine samples were dissolved in 0.5 ml of PBS and subjected to overnight dialysis (500 ml of PBS), to eliminate certain film-forming components that interfere with CryoEM visualization. 3 μl of the sample was deposited on 200 mesh Quantifoil R2/2 grids (spi supplies), which were previously glow discharged with positive charge at 20 mA for 60 s (GloQube, Quorumtech) and plunge-frozen using a Vitrobot Mark IV (Thermo Fischer Scientific). Grids were imaged using a Glacios ThermoFisher cryo-TEM (Thermo Scientific), aligned for parallel illumination, and operated at 200 kV, with the specimen maintained at liquid nitrogen temperatures. Images were recorded on a Falcon 3EC (DED, Thermo Scientific), operated in counting mode with a physical pixel size of 0.95 Å at 150,000 magnification. The total exposure time was 41 s with an accumulated dose of 40 e /$Å^2$ and a total of 38 frames per image.

2.2.4. Dissolution profiles

The dissolution time of the mucoadhesive films was evaluated using an innovative cell for the release of films [32]. The device is composed of a flow-through cell with two chambers separated by a membrane. In the donor chamber, a film was placed and firmly fixed with the edges of the flow cell. During evaluation, a film was in continuous contact with the membrane. A custom-made, constant leveling device provided a steady hydrostatic pressure of the dissolution medium to the flow cell. The system held a constant hydrostatic pressure in both chambers of the flow cell. The dissolution medium (0,1 M phosphate buffer, pH 5,8), simulating saliva, was drained through the donor chamber and the acceptor chamber, resulting in the dissolution of the mucoadhesive film. The system was preheated to 37 °C and the temperature in the flow cell was recorded at one-second intervals, allowing detailed temperature monitoring. The laminar fluid flow design and chamber configuration naturally prolong dissolution times compared to other methods, which allows for the detection of minor differences between formulations. We compared the in vitro release profile of films containing a backing layer and those films without. Samples were collected with an autosampler to determine the fluorescence intensity. Sampling was performed at four-minute intervals. We prepared and compared mucoadhesive films, both with and without a backing layer, containing red fluorescent protein (RFP) as the active agent due to its easy detectability and straightforward assessment. Each film, measuring 2×3 cm, contained an average of 2 mg of isolated RFP protein (determined with UV spectrophotometer). Fluorescence intensity of samples collected with autosampler were measured using a microplate reader (Synergy Mx, BioTek). Samples were excited at 584 nm, and fluorescence emission was measured at 604 nm. To determine the protein concentration and the quantity of released RFP from the film, we compared measured fluorescence intensities with those of a known concentration of RFP, determined via spectrophotometry and the BCA method. A standard curve of fluorescence intensity versus RFP concentration was generated using these measurements. The results are presented as a percentage of the total amount of protein released from the film at different time points. All values were subtracted from blank film absorbance.

2.2.5. Preparation of recombinant proteins

Red fluorescent protein was produced in *E. coli* strain NiCO21 (DE3), which was grown at 37 °C in LB media supplemented with antibiotics at 160 rpm overnight. The inoculum was diluted to 0.1 OD in 1 l of LB media supplemented with antibiotic and left growing at 37 °C before reaching OD values between 0.6 and 0.9, the culture was then induced with 1 mM isopropyl-thiogalactopyranoside and grown for another 4 h at 30 °C. The cell pellet was resuspended in 10 ml per litre of the culture of lysis buffer (50 mM Tris-HCl (pH 8), 150 mM NaCl, Benzonase (Merck), CPI (Protease Inhibitor Cocktails, Millex Sigma-Aldrich). Cells lysis was performed by ultrasonication with a Vibra-cell VCX (Sonics, CT, USA). The cell lysate was purified using Strep-trap (Cytiva, USA),

according to the manufacturer's recommendations. After binding and washing the protein was eluted with 2.5 mM d-Desthiobiotin following the size-exclusion chromatography.

2.2.6. Cell culture and transfection

The human embryonic kidney (HEK) 293 cell line was cultured in DMEM (Invitrogen, Waltham, MA, USA) supplemented with 10% FBS (BioWhittaker) at 37 °C in a 5% CO_2 environment. Mouse NIH-3 T3 cell (ATCC, Manassas, VA, USA) line was cultured in DMEM (Invitrogen, Waltham, MA, USA) supplemented with 10% FBS (BioWhittaker) at 37 °C in a 5% CO_2 environment. For cell infection, mucoadhesive films were placed in the seeded cell culture (12 well plates, $3*10^5$ cells/ml; 1 MAF with 4 mm diameter/well). Mucoadhesive films exhibit the characteristic of floating within the cell medium. Active ingredients, such as mRNA/LNP or viral vectors incorporated into the polymeric matrix are released as the film gradually dissolves. We did not observe any significant cell death caused by the presence of the film components. Cells were harvested after 24 h. As a positive control GFP-pcDNA3 (500 ng/well) was transfected using PEI as transfection reagent. Fluorescence was measured on the 3-laser Aurora spectral flow cytometer (Cytek Bioscience).

2.2.7. Preparation of DNA and mRNA constructs

All plasmids were constructed using the Gibson assembly method or purchased commercially (Promega). We used plasmid pcDNA3 (Invitrogen) as a plasmid backbone. mRNA was prepared from pDNA with a T7 RiboMax Express Large Scale RNA kit (Promega) under the manufacturer's instructions. We used purified PCR fragments for DNA templates, with encoded polyA tail. After DNaseI treatment of the IVT reaction mix, we performed capping of mRNA, using the Vaccinia capping system (NEB M2080S). mRNA was purified according to the manufacturer's instructions with NEB's Monarch RNA Cleanup Kit (NEB T2040L).

2.2.8. mRNA/LNP preparation and quantification

Lipid nanoparticles, encapsulating mRNA, were prepared by Precision Nanosystems Ignite microfluidic mixing platform. Lipid components with a final lipid concentration of 12.5 mM were prepared in ethanol at molar ratios of 50.5:10:38:1.5 (MC3/DSPC/Cholesterol/DMG-PEG2000) and mRNA concentration of 0.200 mg/ml in 25 mM citrate buffer with pH 4.0. The solutions were injected into the NxGen cartridge at flow rate ratios 1:3 with a final flow rate of 12 ml/min. The quantitation of mRNA was performed with the QuantiFluor® RNA System (Promega) with fluorescent RNA-binding dye (492 nm/540 nm). The dye was prepared according to the manufacturer's instructions. The standard was diluted to obtain a linear RNA standard curve. BNT162b2 MAF with a diameter of 4 mm was dissolved in 200 μl of PBS. A control solution of BNT162b2 was diluted in PBS to approximately 20 ng/μl of mRNA. 10 μl of each sample was mixed with RNA binding dye and read on a fluorometer. Absorbance measurements were taken at the appropriate excitation and emission wavelengths (492nmEx/540nmEm) using the multiplate reader SineryMx (BioTek, Winooski, VT, USA). BNT162b2 mRNA/LNP vaccine doses against the SARS-CoV-2 ancestral strain that remained unused were used, based on the approval of the Medical Ethics Board of Slovenia and local authorities at Regierung Oberbayern, Munich, Germany.

2.2.9. Luciferase assays

Luminescence measurements were made using an Orion II microplate reader (Berthold Technologies) with Simplicity software v.4.2. For endpoint luminescence measurements, HEK293T cells were harvested and lysed in 25 μl of 1× Passive Lysis buffer (Promega). Firefly luciferase activity was measured using the luciferase assay (Promega).

2.2.10. Viral vectors

2.2.10.1. Cells lines. HEK293T, DF-1 and A549 cells were maintained and cultivated in Dulbecco's MEM (DMEM) supplemented with 10% Fetal Calf Serum (FCS) and 1% Penicillin/Streptomycin (Pen/Strep) at 37 °C and 5% CO_2 in a humidified incubator. For the generation of recombinant modified vaccinia Ankara (MVA), the AGE1.CR.pIX cell line was used (ProBioGen AG, Berlin). Adherent AGE1.CR.pIX cells were maintained in DMEM-F12 medium supplemented with 5% bovine serum (γ-irradiated, Sigma Aldrich/Merck, 12003C) and 2 mM GlutaMAX I (10565–018).

2.2.10.2. Generation of recombinant MVA. In this study, MVA CR19 was used as a parental MVA strain [33,34] MVA CR19 eGFP was generated by integrating eGFP under the transcriptional control of the early/late modified H5 promoter (mH5) into the thymidine kinase (TK) locus (J2R) of MVA via homologous recombination. Briefly, the antigen-expressing eGFP was cloned into the shuttle vector pMVA Trans-TK containing homologous sequences to the MVA genome and the reporter gene β-galactosidase (β-Gal) between the two left-arm sequences of the TK locus for screening of recombinant MVAs. For in vivo recombination, adherent AGE1.CR.pIX (1×10^6 cells) were infected with parental MVA CR19 with different MOIs ranging from 0.5 to 0.006, incubated for 2 h, followed by transfection with 0.4 μg of the shuttle vector pMVA Trans-TK-eGFP using Effectene (Qiagen, Hilden, Germany) according to the manufacturer's instructions. After 48 h, the cells were harvested and lysed by three freeze-thaw cycles and sonication. Pure recombinant MVAs were separated from the parental MVA CR19 strain by sequential agarose plaque purification based on blue-white screening. The MVA seed stock was generated by large-scale infection of AGE1.CR.pIX cells, cell lysis via three subsequent freeze/thaw cycles and sonification followed by purification via two ultracentrifugation rounds over a 35% sucrose cushion. The titer of MVA CR19 TK-eGFP was determined using crystal violet staining on DF-1 cells. The sequence of the rMVA and absence of non-recombinant MVA were confirmed using PCR amplification, followed by Sanger sequencing. The expression of eGFP was confirmed by Western blot analysis in HEK 293 T cells infected with a MOI of 2 and harvested after 24 h.

2.2.10.3. Generation and titration of adenoviral vector. The E1/E3 deficient adenoviral vector of serotype Ad19a/64 (rAd) was generated as previously described [35]. Briefly, the eGFP antigen was cloned into the shuttle vector pO6-19a-HCMV-MCS under the control of an HCMV promoter. Then, this plasmid was transferred via Flp-recombination in *E. coli* into a BAC vector, which contains the genome of the E1/E3 deleted replication-deficient Ad19a/64-based vector. After restriction digestion of the purified BAC-DNA using *Pac*I the recombinant viral DNA was obtained. The linear DNA was transfected into HEK293T cells for virus propagation. The Ad19a/64-based vector was extracted from the cells via the addition of sodium deoxycholate. By DNase I treatment the residual DNA was removed. The recombinant Ad19a/64-eGFP vector was purified via CsCl gradient ultracentrifugation followed by a buffer exchange to 10 mM Hepes pH 8.0, 2 mM $MgCl_2$ and 4% sucrose via PD10 columns (GE Healthcare, Chicago, USA). The titer was determined using the RapidTiter method by detection of infected HEK293T cells via immunohistochemical staining with anti-hexon antibody (Novus, Adenovirus Antibody (8C4)). The sequence of the antigen was confirmed by PCR amplification using purified vector DNA followed by Sanger Sequencing.

2.2.11. Mouse immunization studies

To test the immunogenicity of the vaccines, female 8–10-week-old BALB/c OlaHsd mice (Envigo, Desio MB, Italy) were used for immunization protocols. All animal experiments were performed according to the directives of the EU 2010/63 and were approved by the

Administration of the Republic of Slovenia for Food Safety, Veterinary Sector and Plant Protection of the Ministry of Agriculture, Forestry and Foods, Republic of Slovenia (Permit Number U34401–6/2021/5). Immunizations were carried out under general inhalation (1.8 MAC isoflurane anesthesia (Harvard Apparatus, Holliston, MA, USA)). If not stated otherwise, the immunization protocol was based on one prime vaccination and one or two boosts with a three-week interval between vaccinations. For the whole duration of immunization, mice were kept on a heating surgical table. The films were placed with Moria forceps onto the buccal mucosa of one cheek, with the mucoadhesive layer facing the buccal mucosa. The animals remained anesthetized for an additional 60 min after the application of the mucoadhesive film to prolong absorption of the vaccine. Intramuscular vaccines were administered using a 30 G needle (Beckton Dickinson, Franklin Lakes, NJ, USA) into *m. tibialis anterior* after appropriate area preparation, given the same amount of mRNA vaccine (3 μg) as determined in one film. For buccal immunization, animals were in general inhalation anesthesia. The animals were left alone for an additional 60 min. For intranasal administration, animals were placed in a mild sedation state. The vaccine was slowly dripped on both nostrils to allow inbreathing of the compound. The maximum volume of the intranasal administration was 20 μl. For the direct gastric delivery, the active compound was dissolved in 50 μl of sterile solution and given into the stomach by direct oral gavage. Administered doses were the same as in MAF for all delivery routes. A negative control group received blank MAFs. One day before each boost, blood was drawn from the lateral tail vein using Microvette 300 (Sarstedt, Newton, NC, USA). Three weeks after the second boost, the experiment was terminated. Subsequently, a final blood sample was collected, and the animals' organs were harvested for further analysis. Mouse sera were obtained by centrifuging blood samples at 3000 rpm for 20 min at 4 °C. The presence of specific mouse antibodies was assessed using ELISA.

2.2.12. In vivo bioluminescence imaging

The mice received 150 mg/kg of body weight of D-luciferin (Xenogen) intraperitoneally and were in vivo imaged with IVIS Lumina Series III (PerkinElmer). Data were analyzed with Living Image 4.5.2 (PerkinElmer). Bioluminescence quantification was presented as total flux, which is presented as photons per second. The values are calculated based on the following equation, having the same area for ROI for all of the animals: Total flux = the radiance (photons/s) in each pixel summed or integrated over the ROI area (cm^2) x 4π. Given slight variation in the size of organs, we take into account the surface area of the mouse when performing analysis and report the results in average radiance instead.

2.2.13. Analysis of immune response in mice

Endpoint titers of designated specific antibodies were determined with ELISA. High-binding half-well plates (Greiner, Kremsmünster, Austria) were coated with recombinant proteins in a PBS buffer (Gibco, Thermo Fisher Scientific, Waltham, MA, USA) at a concentration of 1.2 mg/ml of protein per well and incubated overnight at 4 °C. The plates were washed with PBS + 0.05% Tween20 (PBS-T) using the ELISA plate washer (Tecan, Männedorf, Switzerland) and blocked for 1 h at RT with 100 μl of ELISA/ELISPOT diluent solution (eBioscience). Serial dilutions of sera were added to the plates, where each dilution presented a certain titer value. In the first row, a 1:100 dilution was added, and then a three-fold dilution was performed with each row and incubated at 4 °C overnight. Specific secondary antibodies (dilution 1:3000), coupled with HRP, were added to wells. For total IgG determination, goat anti-mouse IgG (H + L)-HRP antibodies (Jackson ImmunoResearch; 115–035-003, West Grove, PA, USA) and goat anti-mouse IgA alpha chain-HRP (Abcam; ab97235) were used. The plates were washed again, and after the addition of the substrate (TMB solution), the reaction was stopped with 0.16 M sulfuric acid. Absorbance measurements were taken using the multiplate reader SineryMx (BioTek, Winooski, VT, USA). Absorbance at 620 nm was used for correction and was subtracted from the absorbance at 450 nm. EPT was determined as the dilution above the value of the cutoff. The cutoff value was determined from the absorbance data of the control animals (vaccinated with blank MAF).

2.2.14. T-cell response on mouse splenocytes

Single-cell suspensions from spleens were obtained using the tissue dissociator (gentleMACS Dissociator), according to the manufacturer's instructions (Miltenyi Biotec, Bergisch Gladbach, Germany). CD8+ T cells from spleen cell suspension were isolated using a mouse CD8a + T Cell Isolation Kit (Miltenyi Biotec; 130–104-075, Miltenyi Biotec, Bergisch Gladbach, Germany), according to the manufacturer's instructions. Cells were isolated based on the negative selection using LS columns, obtaining up to 10^8 labeled cells. To determine Spike-specific cytotoxicity, mouse NIH-3 T3 cells were seeded into 24-well plates (1×10^5/well); 24 h later, the cells were transfected with pCG1-hACE2 (900 ng/well) and pCMV-TMPRSS2 (30 ng/well) plasmids. The following day, cells were infected with spike pseudovirus with a bioluminescent reporter. The day after, isolated CD8a + T cells (1×10^5/well) were added. Bioluminescence was determined 24 h later using IVISIII (Perkin Elmer, Waltham, MA, USA) after the addition of D-luciferin (500 μM), showing the state of the Spike-specific cytotoxicity of the $CD8^+$ T cells isolated from vaccinated animals. Bioluminescence values are presented as an average radiance (p/s/cm2/sr), which were determined using Living Image® software. The percentage of infected NIH-3 T3-specific lysis was calculated using the following formula: % specific lysis = 100 × (test ARV/maximal killing ARV).

2.2.15. Production of SARS-CoV-2 pseudotyped viruses

To produce SARS-CoV-2 pseudovirus based on the vesicular stomatitis virus, HEK293T pseudovirus-producing cells were transfected with pCG1-Spike. For the SARS-CoV-2 pseudovirus assay, one-day pre-transfection HEK293 cells were seeded (2.5×10^4 per well) in a 96-well plate in DMEM +10% FBS medium. Transfection with a pCG1-hACE2 plasmid (0.02 μg) and a plasmid encoding Renilla luciferase phRL-TK (Invitrogen) was carried out using Lipofectamine 2000 (Invitrogen). Tested compounds were incubated with pseudovirus for 30 min before adding to the cells. The medium was removed the following day, and the cells were lysed in a Passive lysis buffer (Biotium). Pseudovirus infection was determined by the activity of firefly luciferase after the addition of luciferin substrate (Xenogen). To observe Renilla luciferase activity for determination and normalization of transfection in SARS-CoV-2 assay, coelenterazine H (Xenogen) was used. A dual luciferase test for SARS-CoV-2 pseudovirus was performed on the luminometer Orion (Berthold Technology).

2.2.16. Surrogate assay of protection of viral infection by immunization

BALB/c mice were immunized with intramuscular prime (BNT162b2 mRNA) and received booster doses through MAF or IM in three-week intervals. Three weeks after the last immunization, the mice were transfected by 30 μl of the plasmid mixture of transfection agent jetPEI-in vivo (PolyPlus) and plasmid DNA (20 μg hACE2, 1 μg TMPRSS2 per animal) via intranasal administration. Twenty-four hours later, animals were intranasally infected with 50 μl of VSV-S pseudovirus. The next day, the mice received 150 mg/kg of their body weight of D-luciferin (Xenogen) intraperitoneally and were in vivo imaged, using IVIS® Lumina Series III (Perkin Elmer, Waltham, MA, USA). The bioluminescence that depicted the state of the pseudovirus infection was determined. The results were analyzed with Living Image® 4.5.2 (Perkin Elmer, Waltham, MA, USA).

2.2.17. Viral neutralization assay

2.2.17.1. Virus strain. SARS-CoV-2 EU1 strain (EPI_ISL_582134) was isolated from a nasopharyngeal swab of a patient during the first COVID-19 wave in March 2020. The virus was further propagated in Vero E6

cells (ATCC-CRL-1586) cultured in DMEM supplemented with 10% fetal calf serum (FCS), 1% penicillin/streptomycin, 200 mmol/L L-glutamine, 1% MEM-Non-Essential Amino Acids and 1% sodium pyruvate (all from Gibbco, Thermo Fisher). A plaque assay was applied to determine the virus titer in plaque-forming units (PFU).

2.2.17.2. Viral neutralization assay. Vero E6 cells were seeded at 1.5×10^4 cells/well in a 96-well plate in a supplemented DMEM medium and incubated overnight at 37 °C and 5% CO_2. Serum samples were diluted 1:25 in culture medium followed by a 5-fold serial dilution. Serum dilutions were mixed with SARS-CoV-2 virus to reach a multiplicity of infection (MOI) of 0.03 (450 PFU/15,000 cells/well), and incubated at 37 °C for one hour to enable virus neutralization. The inoculum was then incubated on Vero E6 cells for 1 h at 37 °C. Afterwards, the sample/virus mix was replaced by medium and cells were cultured for 24 h. As the positive control, cells were infected with the same MOI of the virus without incubating with serum samples, whereas uninfected Vero E6 cells represent mock. To stop the infection, the cells were rinsed once with PBS and fixed with 4% paraformaldehyde (ChemCruz) at RT for 15 min. After an additional PBS wash, fixed Vero E6 cells were permeabilized for 15 min at room temperature with 0.5% saponin (Roth) in PBS and blocked with PBS with 0.1% saponin and 10% BSA (Roth) overnight at 4 °C. The next day, VeroE6 cells were incubated for 2 h at room temperature with a 1:1500 dilution of SARS-CoV-2 nucleocapsid antibody T62 (Sino Biological, Cat.No. 40143-T62) in PBS supplemented with 1% FCS. Cells were rinsed with wash buffer (PBS supplemented with 0.05% Tween-20 (Roth)) and incubated for one hour at room temperature with goat anti-rabbit IgG antibody, HRP conjugate (Merck KGaA, Cat. No. 12–348) 1:4000 diluted in PBS / 1% FCS. After thorough washing, 100 µl TMB substrate (Invitrogen) was applied to each well and incubated at RT for 8 min in the dark. The reaction was stopped by adding 50 µl of 2 M H_2SO_4 (Roth) and colorimetric detection was performed on an Infinite F200 multiplate reader (Tecan Group AG) at 450 and 560 nm. The data was fit to a log(inhibitor) vs. response model with a variable slope in Prism v 9.2. (GraphPad).

2.2.18. Flow cytometry staining procedure

Cells ($4–5 \times 10^6$ for spleen) were resuspended in FACS buffer (150 µl, PBS supplemented with 10% FBS). For Live/Dead staining, ZombieNIR dye was used according to the manufacturer's protocol. Briefly, FACS buffer was replaced with 100 µl PBS containing ZombieNIR dye (dilution 2000 to 5000). Samples were incubated for 10–15 min on ice, the reaction was stopped with the addition of FACS buffer (100 µl). The ZombieNIR dye was removed with centrifugation at 450 rpm and collected cells were resuspended in 50 µl FACS buffer containing 2 µl Mouse TrueSatin FcX (BioLegend) or anti-mouse CD16/CD32 (Fcy III/II receptor) (BD Pharmingen). Ten minutes later, an antibodies cocktail was added (50 µl) to the mixture and samples were incubated for at least 30 min on ice. The antibody cocktail was prepared in FACS buffer containing 5 µl True Stain Monocyte blocker (426103, BioLegend). See Supplementary Tables 1 and 2 for a list of the antibodies used in this study. Before analysis cells were washed with FACS buffer and fluorescence was measured on the 3-laser Aurora spectral flow cytometer (Cytek Bioscience). All antibodies were titrated individually according to standard practice before being used in the panel. The elevation of distinctive markers was based on phenotyping.

2.2.18.1. Preparation of reference controls. As reference controls, an unstained sample and, for every colour, a single-stain reference control were acquired. All reference controls underwent the same protocol as fully stained samples, including washes. Reference controls were acquired once and used for unmixing the multiple batches. For all parameters, a cell type of interest was used.

2.2.18.2. Data acquisition and analysis. Data were acquired and unmixed using SpectroFlo v3.1.0 software (Cytek Bioscience) using the same instrument settings every run [36]. The resulting unmixed FCS files were analyzed using manual gating in FlowJo v software (BD Biosciences) according to the gating strategy in Fig. S1 and S2. First, a manual data check was performed to ensure the exclusion of technical artefacts and bad-quality samples (clogs, doublets and dead cells). The unmixing of raw data was performed using single-stain controls as references (no manual compensation was used). FlowAI software was used to exclude noise, anomalies in flow rate, signal acquisition and outlier events (REF). Next, doublets and dead cells were removed, and CD45 positive cells were gated manually, subsampled using the FlowJo_Downsample function and saved as new FCS 3.1 files. Before dimensionality reduction and clustering the new files were merged using the FlowJo_Concatenation function. The manually gated cells were further analyzed using the UMAP dimensionality reduction method and X-shift/FlowSOM clustering approach.

For T cells dimensionality reduction: CD4, CD8, CD62L, MHCII, CD103, CD11b, CD44, CD86 and CD69 markers were used; for B cells: MHCII, CD62L, CD44, CD86, CD161, CD11c and for the rest of cells: CD103, CD44, CD4, CD62L, CD11c, MHCII, CD11b, CD8a, CD64, Ly6C, CD86, CD69. FCS files are available upon request.

2.2.19. Statistical analysis

The results are presented as an average ± SEM or SD or using individual data points on a plot. One-way ANOVA was used to determine statistical significance, using GraphPad software (GraphPad Prism 8.4.3 version for Windows, GraphPad Software, San Diego, California, USA).

3. Results

3.1. Formulation of a bilayer mucoadhesive film for trans-buccal vaccine delivery

Mucoadhesive films are thin, flexible matrices composed of polymers that adhere to moist biological surfaces such as buccal membranes. They are usually composed of natural and biodegradable polymers with bioadhesive properties to improve bioavailability by prolonging retention time at the application site. MAF should maintain a stable vaccine formulation and withstand mechanical stress during handling and application [37,38]. In this study, we evaluated MAFs comprising water-soluble polymers, where all active ingredients were water-soluble. This ensured compatibility and uniform distribution of the active ingredients throughout the film matrix, without compromising their functionality. The polymeric matrix of the mucoadhesive layer was prepared by blending trehalose, pullulan, and sucrose in a PBS solution which upon drying solidified into a homogenous film. Pullulan is used for tablet coating, in the production of edible films, and has an excellent film-forming ability. Trehalose and sucrose are most commonly used in the food industry, known for their stabilizing capacity. Pullulan and trehalose can form thin, uniform films when dissolved in aqueous solvents. This film-forming ability facilitates the easy preparation of mucoadhesive films and allows for precise control over film thickness and drug loading. Furthermore, the combination of these polymers has great mucoadhesive properties, it can adhere to mucosal surfaces upon contact. This adhesive interaction promotes prolonged contact between the film and the mucosa, enhancing drug absorption and bioavailability. The spreadability, flexibility and elasticity of the mucoadhesive films were improved by the addition of glycerol into the final mixture. To prevent the undesired loss of active agents to the saliva, the side of the film facing the mouth cavity was layered with a protective and water-insoluble ethyl cellulose layer to ensure the unidirectional antigen release towards the buccal mucosa (Fig. 1B). Ethyl cellulose is commonly used as a polymer for backing membrane with the addition of plasticizer, such as diethyl phthalate to impart flexibility of the film and retain it during the storage. The mucoadhesive films were prepared using the solvent-casting method and were cut into individual units

measuring 2 cm × 3 cm or punched into circular units with a diameter of 4 mm for animal immunization (Fig. 1C **and** Fig. 1D). Prepared films were stored individually in metalized polyester or aluminum foil or in a petri dish. Bilayer film cross-section morphology was evaluated by scanning electron microscopy (SEM), where both layers were smooth and distinguishable. SEM images indicated homogenous and densely packed layers. The resulting films had smooth surfaces and showed no signs of defects or layer separation. The mucoadhesive layer of the film had an average thickness of 400 μm, while the backing layer had an average thickness of 30 μm (Fig. 1E). A thicker mucoadhesive layer could increase the retention time of the mucoadhesive film and enclose a higher amount of incorporated active ingredients. However, thicker film might also be more prone to detachment from the mucosa. To improve long-term stability and facilitate easier handling, additional layers may be incorporated [39–41].

3.2. Dissolution profiles for mucoadhesive films, containing a backing layer

The addition of a backing layer is an efficient way to provide controlled, unidirectional release of active agents by acting as a barrier that prevents its dissolution into the saliva and its loss by saliva ingestion. It prolongs the film's attachment to the mucosal surface and enhances antigen penetration [42,43]. To evaluate the impact of the backing layer on the dissolution time of the film, we conducted studies using a flow-through dissolution device [44]. We compared mucoadhesive films, both with and without a backing layer, incorporating RFP as the active ingredient. We observed distinguishable differences in the rate and time of dissolution (Fig. 1F). After 30 min, MAF without a backing layer released >95% of the RFP, whereas MAF with the backing layer exhibited a prolonged release, resulting in a slower dissolution rate compared to films without a backing layer. Films with a backing layer released approximately 80% of the RFP in 90 min. Films without a backing layer exhibited a higher release rate and greater water uptake capacity due to their ability to absorb water from both directions. In contrast, the mucoadhesive bilayer film showed a slower dissolution rate, as a consequence of water uptake from only one side, which slowed the protein release rate and prolonged the presence of the protein at the administration site and the amount of active ingredient delivered to the mucosa. To confirm the impermeability of the ethyl cellulose backing layer, we inverted the bilayer film to expose the water-impermeable layer towards the release medium. In this case, the film released about 10% of the RFP in the first few minutes, mainly due to the lateral release of proteins at the edges of the film. Afterwards, the amount of released protein remained constant for over an hour, confirming that the backing layer was not leaking. Results highlight differences in dissolution profiles of formulations with and without a backing layer.

3.3. Delivery of viral vector-based vaccines via mucoadhesive films and assessment of short-term stability

Viral vectors are capable of inducing strong and comprehensive (cellular and humoral) immune responses and are efficient vehicles for ectopic expression of therapeutic genes in target cells or tissues [45,46]. To investigate the delivery capabilities for vectored vaccines by MAF, we used recombinant adenoviruses (AV) [47,48] and modified vaccinia Ankara (MVA) [49] encoding enhanced green fluorescent protein (eGFP) and compare their ability to infect cells. Feasibility tests were conducted on HEK293 mammalian cell lines to assess the release of MAF-formulated viral vectors. Films were added to the cell culture medium, where they gradually dissolved and allowed cell infection. As a positive control, cells were transfected with a liposomal mixture containing an expression plasmid for eGFP (500 ng) and as a negative control a film without a viral vector (blank film) was dissolved in the medium of seeded cells. Twenty-four hours later we analyzed the fluorescence intensity of expressed GFP in the mammalian cells. Our findings confirmed the successful release of functional viral particles (MVA and AV) from the polymeric matrix of the film and the infection of cells in the culture. This observation demonstrated that the viral vectors retain their activity when incorporated and released from MAF (Fig. 2A). Next, the MAF containing either eGFP-MVA (4×10^4 IU) or eGFP-AV (1×10^5 IU) were administered to buccal mucosa of mice. In vivo bioimaging of eGFP performed 24 h after application of films revealed the highest GFP expression in the local area around the oral cavity, indicating effective delivery and gene expression in the targeted region (Fig. 2B left and **Supp. Fig. 1A**). To assess whether viral vectors withstand the process of film preparation and short-term storage, films containing viral vectors were stored at 4 °C or room temperature for 7 days before conducting the same experiments. The results demonstrated that the film-formulated viral vectors (MVA and AV) remained stable for at least one week at refrigerator temperatures (4 °C). While AV particles retained their infectivity even after storage at room temperature for one week, the infectivity of MVA-film gradually decreased over time at this temperature (Fig. 2B right). This result is consistent with the reports that non-enveloped viruses tend to be more stable than enveloped viruses [50].

To confirm that viral vectors are delivered through the oral mucosa and not through the lower gastrointestinal tract, we compared organs from animals, that were given eGFP-MVA by oral gavage (oral), through MAF via buccal mucosa (MAF buccal) or dissolved MAF by oral gavage (MAF oral) (Fig. 2C). GFP fluorescence in the stomach was significantly lower in the group receiving a buccal application of MAF than in the group receiving viral vector orally, stipulating that eGFP-MVA is indeed absorbed through the buccal mucosa by film delivery (Fig. 2D). Additionally, we immunized animals with GFP-MVA and compared the response of buccal administration of MAF with the same amount of the virus administered to the buccal tissue without the film. After 2 days, animals were imaged to detect GFP expression in the whole mouse and in the mucosal region (**Supp. Fig. 1**). The results demonstrate that with MAF delivery, local absorption occurs, and the response does not originate from the ingested active ingredients. Importantly, MAF enhances absorption compared to the formulation delivered without the film.

A concern associated with mucosal delivery is the potential migration of viral vectors to the central nervous system (CNS) via the olfactory epithelium [51]. Vaccine components could be transported via the trigeminal nerve to the brain where they could potentially induce adverse effects [5,52]. To evaluate the ability of the active agents to reach the brain, one group of animals received GFP-MVA intranasally (IN), the second group received GFP-MVA orally (oral), and the third group was immunized through the buccal mucosa with MAF. Twenty-four hours after immunization, we performed fluorescent brain imaging to evaluate the extent of GFP expression in each group (Fig. 2E). MVA does not cause neural damage even after intracranial inoculation [53,54]. This highly attenuated virus furthermore cannot replicate in most mammalian cells and was reported not to gain access to the brain after intranasal application [53]. This property may explain the substantial scatter in our results where we aimed to detect the translation of a viral reporter rather than infectivity. The amount of detected GFP and differences between the groups did not reach statistical significance. GFP fluorescence was observed in the brains of two out of five animals in the group receiving intranasally administered GFP-MVA in one animal in the oral group and no animal exhibited fluorescence in the MAF group.

3.4. Vaccination concept with AV-based vector delivered via mucoadhesive films

To assay the immunogenicity of the described vaccination platform, we investigated the production of neutralizing antibodies against SARS-CoV-2 as proof of principle. For this study, an adenoviral vector encoding the receptor binding domain (RBD) of SARS-CoV-2 fused to the oligomerizing beta annulus domain (RBD-bann) was formulated into MAFs. It has been demonstrated in a prior study that mice immunized

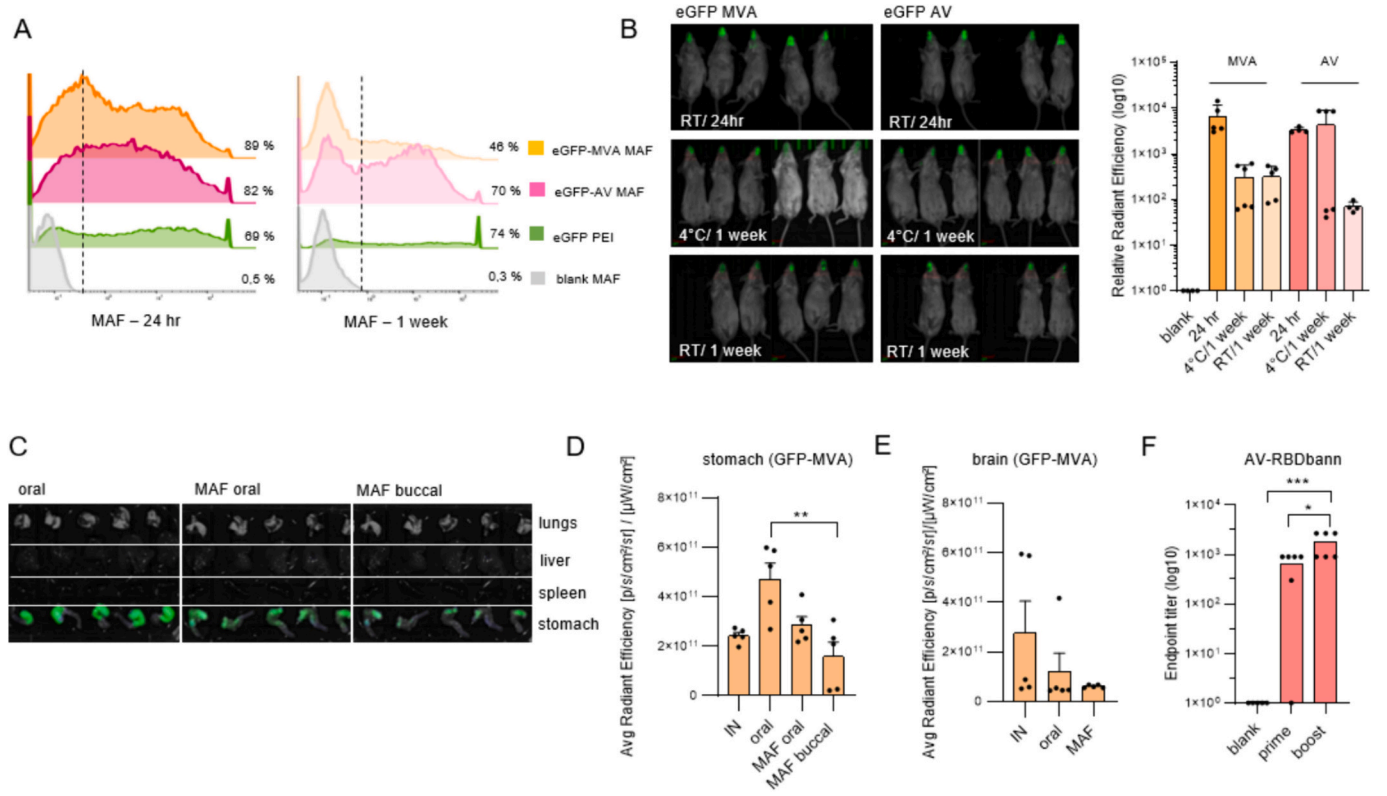

Fig. 2. Stability of viral vector vaccines and comparison of different types of nucleic acid delivery applications. (**A**) The histogram profiles show eGFP expression in HEK293 cells infected with MAF containing eGFP-AV (1×10^5 IU per film) or eGFP-MVA (4×10^4 IU per film). The MAFs were stored for 24 h or one week. Cells were analyzed by flow cytometry. As a positive control cells were transfected with transfection reagent and pDNA encoding eGFP; (**B**) In vivo delivery of MVA and AV encoding eGFP via MAF stored under three different conditions: 24 h at RT, one week at RT, and one week at 4 °C. Twenty-four hours after administration of MAF, mice were subjected to fluorescence imaging (left). The intensity of eGFP is presented as an average radiant efficiency with SD. Each dot represents an individual animal (right); (**C**) MVA-mediated eGFP expression in murine organs after oral intake of GFP-MVA (oral), oral intake of dissolved MAF (MAF oral) and buccal delivery of MAF (MAF buccal) ($n = 5$); (**D**) MVA-mediated eGFP expression in murine stomach after intranasal delivery of eGFP-MVA (IN), oral intake of eGFP-MVA (oral), oral intake of dissolved MAF (MAF oral), and buccal delivery of eGFP-MVA via MAF (MAF buccal). The intensity of eGFP was measured 24 h after the administration and presented as an average radiant efficiency [p/s/cm^2/sr]/[µW/cm^2] and SEM. Significance was tested with one-way ANOVA with Tukey's comparison. $^{**}p < 0.01$ (n = 5); (**E**) The expression of eGFP in the murine brain was measured after intranasal delivery of eGFP-MVA (IN), oral ingestion of eGFP-MVA (oral), and MAF delivery (MAF). The intensity of eGFP was measured 24 h after the administration and presented as an average radiant efficiency [p/s/cm^2/sr]/[µW/cm^2] with SEM; (**F**) Immunization of BALB/c mice with MAF with AV-based vectors encoding Spike-RBDbann of SARS-CoV-2. Spike-specific serum IgG response was determined three weeks after the prime dose and three weeks after the booster dose. Statistically significant differences are indicated among groups receiving blank MAF without viral vector and a group receiving AV-MAF. Each dot represents an individual animal. $^{*}p < 0.1$, $^{***}p < 0.001$. All *p*-values were obtained from a one-way ANOVA followed by Tukey's multiple comparison tests.

with RBD-bann not only developed a robust T-cell response but also exhibited significantly higher antibody titers compared to mice immunized with monomeric RBD [55]. Films, containing AV-RBDbann were applied to the animal buccal mucosa to evaluate the immunogenicity of MAF vaccines and assess whether viral vectors packed in the delivery vehicle can elicit a robust antigen-specific humoral immune response. The animals received two immunizations based on film AV-RBDbann vaccine delivery with a three-week interval between the doses. The results indicate that mucosal immunization through MAF-induced RBD-specific IgG endpoint titers within three weeks after a single vaccination, which was further increased by the booster dose (Fig. 2F). We concluded that immunization with AV-RBDbann via MAF elicits a robust antibody response, supporting further development of viral vectored mucosal vaccines.

3.5. Delivery of mRNA/LNP vaccines via mucoadhesive films

Lipid nanoparticles (LNPs) emerged as a potent delivery system for encapsulated nucleic acid-based therapeutics such as mRNAs for therapy or vaccination [56–59]. A prolonged and efficient topical delivery to enable presentation to dendritic cells is highly desirable for shaping a strong immune response [60]. To confirm the structural integrity of lipid nanoparticles even after the polymeric matrix solidified into the mucoadhesive film, the LNP-containing MAFs were dissolved and analyzed by cryo-EM. The results confirmed that the LNP structure remained intact even after the polymeric matrix solidified into the film and after its dissolution (Fig. 3A). Further we measured the quantity of mRNA in LNPs formulated in MAF. We compared the mRNA content in the film-incorporated LNPs with mRNA/LNP that was not incorporated into the films. We observed a 33% loss of mRNA when stored at room temperature for one month and a 17% loss of mRNA compared to fresh films when stored in the refrigerator. The observed mRNA degradation was similar to the mRNA/LNP, which was not formulated into the mucoadhesive films (Fig. 3B), demonstrating that incorporation into the MAF does not affect its stability. Moreover, in vivo studies conducted with BALB/c mice supported the effectiveness and retention of bioactivity of mRNA/LNPs delivered through mucoadhesive films. The application of MAF-containing mRNA/LNP encoding fLUC to the buccal mucosa resulted in the expression of firefly luciferase, demonstrating the potential for the mucosal administration of mRNA/LNP-based vaccines (Fig. 3C).

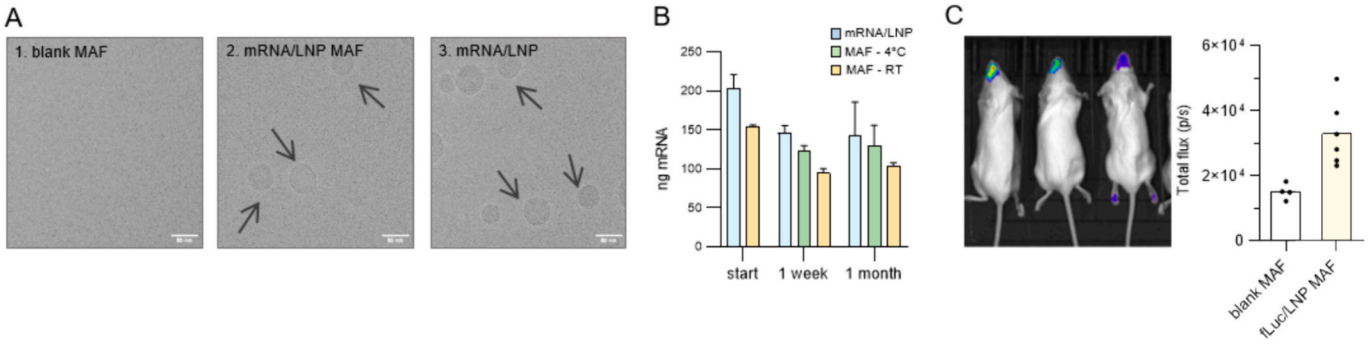

Fig. 3. MAF-mediated delivery of mRNA/LNP vaccines. (**A**) CryoEM images displaying blank MAF dissolved in 150 mM NaCl (1), MAF containing mRNA/LNP (3 μg of BNT126b2) dissolved in 150 mM NaCl (2), and mRNA/LNP diluted in 150 mM NaCl (3). LNPs are indicated with arrows. The scale bar represents 50 nm; (**B**) Assessment of storage stability of mRNA/LNPs (3 μg of BNT162b2) formulated in MAF at the start of the experiment, one week and 1 month later, stored at room temperature or 4 °C in comparison to mRNA/LNP, which was not formulated into the MAF (200 ng); (**C**) In vivo delivery of mRNA/LNP encoding fLuc (5 μg of mRNA) via MAF onto the buccal mucosa of mice. Bioluminescence imaging was performed 24 h after MAF administration.

3.6. Heterologous vaccination regime with mRNA/LNP-MAF encoding SARS-CoV-2 Spike protein

To determine the efficacy of booster vaccination through the oral mucosa, BALB/c mice were immunized with mRNA/LNP (3 μg of mRNA) encoding the SARS-CoV-2 spike protein with prime dose followed by two booster doses spaced 21 days apart, given by either IM, MAF or IN (Fig. 4A). We expected that the IM prime dose would induce a systemic virus-specific IgG response, while the mucosal vaccine would induce the production of specific IgAs, providing additional protection

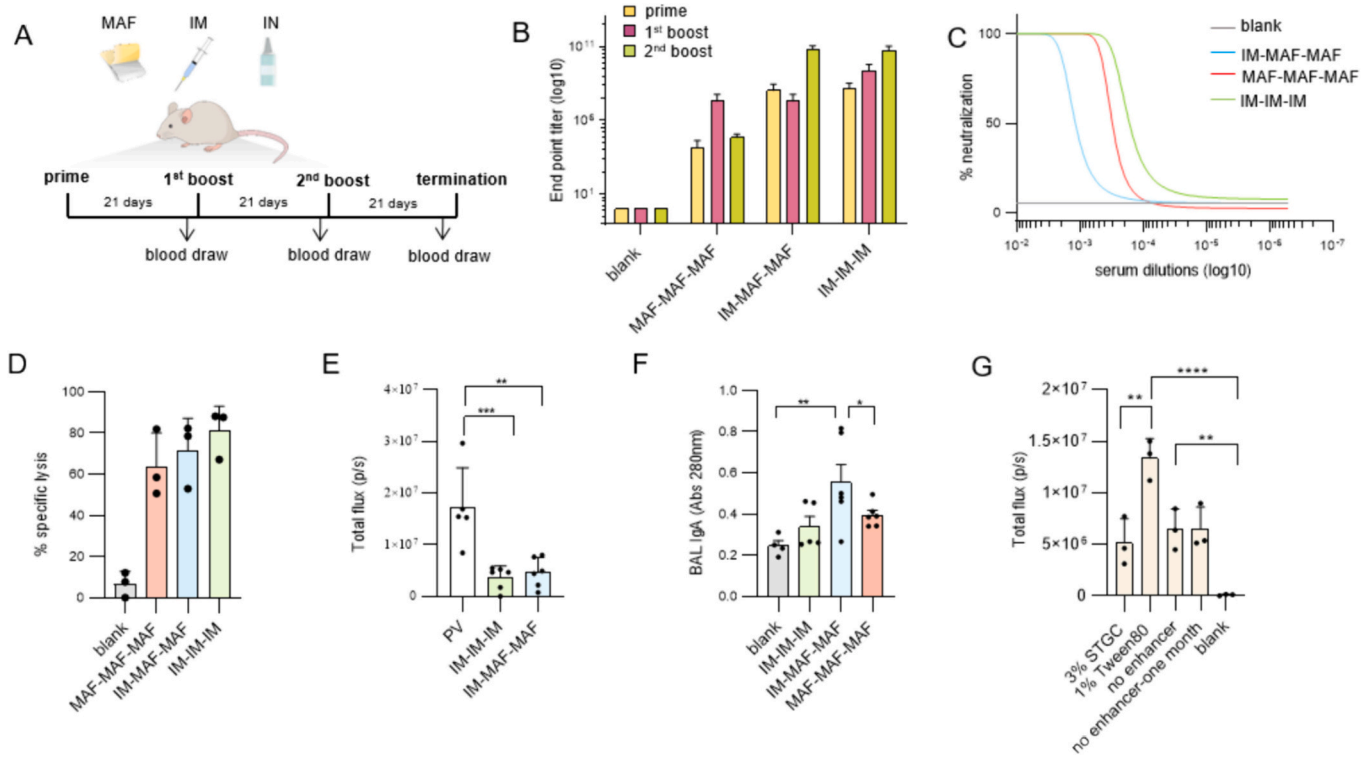

Fig. 4. Immunization of mice with mRNA/LNP encoding SARS-CoV-2 Spike protein and plasmid DNA delivery. (**A**) Schematic representation of vaccination regime and time points of sample collection. BALB/c mice were immunized with mRNA/LNP vaccine, followed by two booster immunizations of mRNA/LNP vaccine via MAF, IN or IM, with a three-week interval between each dose; (**B**) Endpoint titers of total IgG antibodies against SARS-CoV-2 Spike protein determined by ELISA three weeks after the prime dose and three weeks after each booster dose (blank $n = 6$, IM-IM-IM $n = 5$; IM-MAF-MAF n = 6; MAF-MAF-MAF n = 6); (**C**) Inhibition of pseudoviral infection of Vero E6 cells by diluted mouse sera (blank n = 6; IM-IM-IM n = 6; IM-MAF-MAF n = 5; MAF-MAF-MAF n = 6). Nonlinear regression was used to fit curves; (**D**) Induction of Spike-specific cytotoxic T cells extracted from the spleens of immunized animals. The isolated CD8+ T-cells were subjected to cytotoxicity assessments using pseudovirus-infected NIH-3 T3 cells transfected with hACE2 and TMPRSS2. The specific lysis of NIH-3 T3 cells was calculated based on radiance values obtained from the pseudoviral infection. Each dot represents spleen cells from an individual animal; (**E**) Mice were exposed to a challenge with a SARS-CoV-2 pseudotyped virus three weeks after the second boost. Luminescence was measured after 24 h. Each dot represents an individual animal (PV n = 5; IM-IM n = 6; IM-MAF n = 6). Statistical significance was observed with $^{**}p < 0.01$, $^{***}p < 0.001$; (**F**) Detection of IgAs against SARS-CoV-2 Spike protein was measured with ELISA three weeks after the second booster dose. Graphs represent the mean and SEM (n = 5). $^{*}p < 0.1$, $^{**}p < 0.01$. All p values are from one-way ANOVA followed by Tukey's multiple comparison test; (**G**) The impact of penetration enhancers on the entry of plasmid DNA into the animal mucosa, as indicated by reporter luciferase expression, is reported as an average with SD. Each animal received one film containing 30 μg of pDNA. Each dot represents an individual animal ($n = 3$). Significance was tested with one-way ANOVA with Tukey's comparison. $^{**}p < 0.01$, $^{****}p < 0.0001$ (n = 3).

in comparison to parenteral immunization. Fig. 4B displays the endpoint titers of Spike IgG antibodies in mouse sera, measured three weeks after the prime and three weeks after each booster immunization. Animals immunized at all three steps with the MAF formulations (MAF - MAF - MAF) showed the formation of antibodies against Spike protein, already after a prime dose and with a response potentiated by booster shots. After administering the first booster dose, the immune response in the group receiving only mucoadhesive films (MAF - MAF - MAF) and the group receiving an intramuscular prime (IM - MAF - MAF) was found to be comparable and upon administering an additional dose, the final titers for the group receiving films (MAF - MAF - MAF) demonstrated a slightly weaker response in comparison to the group with parenteral priming (IM - MAF - MAF). After the final boost, the EPTs for the group receiving three intramuscular doses (IM - IM - IM) were comparable to the group boosted with the film (IM - MAF - MAF). These results suggest that combining the MAF boosters with IM prime immunization exhibits an immunological response comparable to the standard vaccination (IM - IM - IM). To further investigate the humoral protection against SARS-CoV-2 infection, we evaluated the production of neutralizing antibodies in serum samples from vaccinated animals using the SARS-CoV-2 pseudotyped VP-based assay (Fig. 4C). All sera from groups IM - IM - IM, IM - MAF - MAF, and MAF - MAF - MAF potently neutralized the fully competent SARS-CoV-2 virus. The group receiving only intramuscular doses exhibited the most potent neutralization, with an IC50 of 1:9000, indicating a high neutralization potency. Interestingly, the group receiving only films (IC50 dilution of 1:3700) showed superior results to IM – MAF - MAF (IC50 dilution of 1:150). We compared our results with an intranasal route of delivery, as an alternative mucosal delivery route. Additional groups included three doses of IN (IN-IN-IN) and IM prime followed by IN boosts (IM-IN-IN). The group receiving only intranasal vaccine demonstrated an absence of neutralizing antibodies (**Supp. Fig. 2A**). This observation is consistent with a previous report where a single-dose of nonadjuvanted IN spike protein alone was not generating IgGs and required prior systemic priming [61]. To demonstrate that the effect of buccal MAF vaccine application indeed proceeded through the transbuccal delivery, we performed additional controls including MAFs dissolved and administered directly into the stomach (MAF stomach), as well as mRNA/LNP formulation applied buccally (mRNA/LNP buccal) and administered directly into the stomach (mRNA/LNP stomach) (**Supp. Fig. 2C**). Results demonstrate that the delivery of vaccine through the stomach or delivery without MAF is substantially weaker than via the buccal delivery of MAF.

Although neutralizing antibody production often correlates with the development of protective immunity, T-cell responses were shown to protect against SARS-CoV-2 even in the absence of neutralizing antibodies. Such protection was observed in natural infection [62] and in a study that investigated intranasally administered MVA-vectored vaccine [63]. We evaluated cytotoxic $CD8^+$ T cellular response by isolating $CD8^+$ cells from immunized mice spleens three weeks after the second boost. Specific augmentation of cell killing was observed upon co-culturing isolated CD8+ T cells with SARS-CoV-2 pseudovirus-infected NIH-3 T3 cells, for groups MAF - MAF - MAF, IM - MAF – MAF, and IM - IM - IM (Fig. 4D). The results of the cytotoxic $CD8^+$ T responses align with the EPTs, showing the most favorable response in the IM - IM - IM group (80% specific cell lysis), followed by the IM - MAF - MAF group (70% specific cell lysis). The group receiving three treatments with MAF exhibited slightly lower specific cytotoxicity. Protection through MAFs was also assessed by the surrogate assay of protection against viral infection by immunization. To test the prime-boost regime in mice, hACE2 and TMPRSS2 were introduced into mice to enable infectivity by SARS-CoV-2 as shown before [55]. Mice were immunized with a prime-boost regime (according to the scheme in Fig. 4A) and challenged with a SARS-CoV-2 pseudotyped virus three weeks after the final boost. The protection against infection was observed in both groups immunized with the IM regime as well as in a group receiving booster doses in the form of mucoadhesive films (Fig. 4E). Those findings confirm that designed films effectively provide in vivo protection against an intranasal infection by a virus that mimics the initial phases of SARS-CoV-2 infection. We showed a robust Spike protein-specific cytotoxic T-cell response was initiated, supporting the generation of neutralizing antibodies and licensing of cytotoxic lymphocytes, which contribute to vaccine efficacy.

The spleens obtained from immunized mice were analyzed by flow cytometry to assess the expression of surface markers. For the group subjected to the MAF-MAF-MAF immunization regimen, we observed an elevated presence of distinctive markers on $CD19^-CD3^-$ cells, including $CD11c^{high}$, MHC II, and up-regulated CD86 (**Supp. Fig. 3 A_12**) [64], which are associated with dendritic cell maturation, responsible for initiating T-cell immunity and directing other antigen-specific immune responses [61,62]. The MAF-MAF-MAF regimen also exhibited induction of $CD4^+$ $CD8^-$ T cells, with a subpopulation expressing $CD62L^{high}$ (**Supp. Fig. 3 B_2 and 4 B_3**), which facilitates migration of leukocyte cells and interactions with dendritic cells [65,66] and different subpopulations of $CD44CD4^+$ T cells, which are upregulated during the response against invading microbes and involved in cell migration, activation and differentiation (**Supp. Fig. 4 B_2**) [67]. Some of these subpopulations are also associated with tissue-resident memory T cells, recognized for their presence in mucosal surfaces and their vital role in local defense against respiratory infections (**Supp. Fig. 3 D_10 and 4 D_2**) [68].

3.7. The combined IM prime and mucosal boost vaccination strategy augments the mucosal immune response

Despite robust induction of humoral and cellular immunity, current COVID-19 mRNA vaccines provoke poor mucosal immunity in the respiratory tract [69]. Especially in the case of airborne viruses like SARS-CoV-2, where the Spike protein interacts with the receptor expressed in the upper respiratory tract epithelium [70], mucosal immunity is required for clearance of the infectious agents and to prevent the establishment of the infection [71]. IgA has a key role in capturing the antigens and other microorganisms in the oral mucosa and preventing epithelial cell infection. Several studies have shown that IgA possesses better anti-viral properties than IgG with serum IgA being more potent than serum IgG in viral neutralization [72]. Therefore, a strong induction of mucosal response is beneficial for the prevention of respiratory infections since the lack of neutralizing anti-SARS-CoV-2 IgA and secretory IgA antibodies represent a possible cause of prolonged viral shedding [73]. Intramuscular delivery of mRNA/LNP elicits primarily IgG response in the serum. The IgA response is however modest and wanes faster than the IgG response [74]. We expected that the mucosal vaccine encoding the SARS-CoV-2 spike delivered via buccal mucosa could induce the secretion of localized IgA within the mucosa, providing additional protection against SARS-CoV-2 compared to IM delivery. Therefore we analyzed the IgA generation by the mRNA/LNP formulations in an immunization scheme in Fig. 4A. Results show that only mice receiving the mucosal booster dose developed high titers of IgA. In contrast, the IgA response was low in the case of the IM regime only (Fig. 4F and **Supp. Fig. 2B**). We observed the highest IgA response in a group receiving a heterologous vaccination combining both IM and MAF. This suggests that a combination of both routes of administration may elicit a more robust mucosal immune response, highlighting the potential benefits of heterologous vaccination strategies in enhancing mucosal immunity and reminiscent of a similar effect that was demonstrated with the simultaneous administration of influenza vaccine by aerosol and IM injection [75]. We demonstrated that mucosal boosters provoked cellular immunity, compelling mucosal IgA, and neutralizing activity against the tested virus.

3.8. Delivery of plasmid DNA by mucoadhesive films

Following the analysis of the MAF delivery of vectored and mRNA/

LNP vaccines, we tested the delivery of DNA plasmid vaccine as a platform to evaluate the delivery potential of MAF. DNA vaccines may be a suitable platform for the delivery with MAF since they do not need to be stored at low temperatures and are cost-effective to manufacture. However, DNA does not possess the same mechanism of uptake and transport across epithelial barriers as lipid nanoparticles and viral vectors, making it less effective at penetrating the epithelium [76,77]. Penetration enhancers could improve tissue permeability and enhance the distribution of DNA within target tissues, thereby improving therapeutic efficacy in comparison to vectored and LNP-delivered agents that can enter cells more readily than plasmid DNA. Permeation of mucosa can be enhanced by chelating agents (EDTA), surfactants (sodium lauryl sulfate), polyols (propylene glycol) or fatty acids (oleic acid) and similar agents [78] in the formulation that cause transcellular perturbations in the oral epithelium [79,80]. The perturbations are rapidly restored due to the short turnover of oral epithelial cells [81]. In our study, MAF containing plasmid DNA (pDNA) encoding firefly luciferase (fLuc) was applied to the buccal mucosa of mice. Successful penetration of pDNA through the mucosa was indicated by the detection of firefly luciferase expression in mice after 24 h, with the highest expression observed in the tissues surrounding the oral cavity. Here, the efficacy of two penetration enhancers, 1% Tween 80 and sodium tauroglycocholate (STGC), was tested. The choice of Tween 80 and STGC as penetration enhancers was guided by prior reports indicating their effectiveness in boosting mucosal permeation. Bile salts are known for their potent penetration-enhancing abilities, attributed to their capacity to disrupt lipid membranes. STGC accumulates in the tissue without causing a loss of superficial cell layers and interacts with the intercellular or membrane lipids thus increasing the permeability of the permeant through the epithelium. At 3% concentration, STGC showed the highest K_p and EF across the buccal mucosa [82,83]. In comparison, the nonionic surfactant, Tween 80 has shown notable permeation enhancement, especially in mucosal delivery contexts by hydrophobic interactions with keratin fibrils causing swelling of the epithelium. A formulation containing 1% Tween 80 was found in our system to be more effective than STGC in enhancing permeation, as evidenced by significantly higher levels of luciferase expression (Fig. 4G). Other permeation enhancers, surfactants, or chelating agents may be explored to further potentiate antigen permeation through the oral mucosa [84]. We found that plasmid-incorporated MAFs can be stored at room temperature for more than a month without loss of activity. Plasmid DNA integrity therefore appears not to be compromised even in the absence of cold-chain transportation (Fig. 4G). Membrane-active permeation enhancers are however not compatible with LNPs or encapsulated vectors as they could affect the integrity of their membranes. Further studies would be needed to explore the feasibility of other penetration enhancers with viral particles or lipid nanoparticles but may be compatible with non-enveloped vectors.

4. Discussion

In this study, we present a mucoadhesive bilayer film platform applied for buccal administration of viral vectors, LNP-packaged mRNA, and DNA plasmids. While oral immunization has been traditionally associated with the loss of vaccines to the gastrointestinal tract, buccal application of MAFs can overcome this limitation.

MAF made from trehalose, pullulan, and sucrose demonstrated good mucoadhesive properties while preserving the biological activity of the incorporated active agents. The additional protective layer made from ethyl cellulose significantly prolonged the film's attachment to the mucosal surface, enhancing antigen penetration and controlled unidirectional release, thus preventing vaccine loss to the oral cavity. Unlike the controlled conditions of a laboratory setup, the oral cavity is subjected to factors such as saliva composition, pH fluctuations, enzymatic activity, and mechanical movements and the results obtained from the dissolution device can only serve as an approximation. For example, a film with dimensions of 2 cm × 3 cm, when placed in 100 ml of 0.1 M phosphate buffer, stirred at 100 rpm, takes only 5 min to dissolve. However, results highlighted the differences in dissolution profiles of formulations with and without a backing layer.

We could confirm in our study that different vaccination platforms for immunization can be used to present antigens to the immune system [85,86]. To address the need for sustained booster strategies that depend on high acceptance and vaccine uptake rates, we propose to explore a heterologous vaccine regime with mucoadhesive films after parenteral priming or previous infection. Mucoadhesive films containing mRNA/LNP used as booster shots generated titers comparable to a standard intramuscular vaccination. They also triggered local IgA titers that could have the potential for improved immune protection against respiratory infections. Furthermore, MAF induced a Spike-specific cytotoxic T-cell response, a property that may be crucial for controlling diseases and reduction of viral shedding, however, the duration of protection mediated by IgA needs to be explored further.

Interestingly, the adenoviral COVID-19 vaccine designed for intramuscular application recently demonstrated good efficacy of intranasal delivery with good IgA response and protection in a mouse model, similar to the sIgA obtained with MAF [87].

The MAF could be further optimized for delivery depending on the incorporated active agent. Further penetration enhancement may be achieved by technologies like mucus-penetrating particles [88] or by a physical modification [89]. Incompatibility of LNP with surfactants as penetration enhancers may be bypassed by an additional mucosa-interacting layer comprising penetration enhancers, that could render oral epithelium more permeable while preventing direct interaction on the active agents in the second layer [78,79]. To further improve the immune response, suitable vaccine adjuvants, bacterial or viral vectors, and LNPs specifically designed for mucosal delivery could also be integrated into the MAF. The development of non-toxic and effective mucosal adjuvant remains the focus of mucosal vaccine development, which could also be integrated into the mucoadhesive film and consequently improve the immune response [5].

The oral epithelium of mice is keratinized, which can affect transmucosal delivery. To address this limitation, future studies would require experiments on animal models with non-keratinized mucosa, such as e.g. rabbits or pigs with an oral mucosal structure more closely resembling humans. Ultimately, clinical studies would be necessary to evaluate the immune response and other relevant parameters, providing crucial insights for the development of transmucosal delivery systems.

The administration of MAF-based vaccines is non-invasive and would not require trained personnel, making it a potentially widely applicable and acceptable alternative, particularly for patient groups, including pediatric, geriatric, and nauseous patients and deployment in the field with less developed medical infrastructure. By providing an efficient and easy-to-implement platform for vaccine and biological drug delivery, mucosal vaccines are expected to improve patient compliance, and accessibility, and provide effective long-lasting protection against various infections.

5. Conclusion

This study has shown that mucoadhesive films can successfully induce local and systemic immune response and that they can be used to deliver different types of vaccine platforms, including viruses, DNA plasmids, and mRNA/LNPs. By complementing the intramuscular priming, this type of vaccine delivery platform could play an important role in achieving sustainable booster strategies with broad implementation and higher acceptance. Mucoadhesive films may enhance vaccine efficacy, promote patient compliance, and reduce the fear sometimes associated with traditional vaccination methods. Given the complexities of mucosal immune regulation and limited access to mucosal inductive sites, mucoadhesive films hold the potential to complement intramuscular vaccination.

Funding

This work was supported by grants from the Slovenian Research Agency [P4–0176, P3–0289]. This work was financed in part by the project Virofight which has received funding from the European Union's Horizon research and innovation program Grant agreement ID: 899619 and Centre for Technologies of Gene and Cell Therapy, which has received funding from the European Union's Horizon research and innovation Teaming program Grant agreement ID: 101059842. The project was also funded by the Slovenian Research and Innovation Agency (projects J3-4526 and J7-4493)

CRediT authorship contribution statement

Hana Esih: Writing – original draft, Methodology, Investigation, Data curation. **Klemen Mezgec:** Methodology, Investigation, Data curation, Writing – original draft. **Martina Billmeier:** Resources, Methodology, Data curation. **Špela Malenšek:** Investigation. **Mojca Benčina:** Investigation, Data curation. **Blaž Grilc:** Investigation, Data curation. **Sara Vidmar:** Investigation, Data curation. **Mirjana Gašperlin:** Resources. **Marjan Bele:** Investigation, Data curation. **Mihaela Zidarn:** Resources. **Tatjana Lejko Zupanc:** Resources. **Tina Morgan:** Resources. **Ingo Jordan:** Writing – review & editing, Formal analysis. **Volker Sandig:** Formal analysis. **Silke Schrödel:** Resources. **Christian Thirion:** Resources. **Ulrike Protzer:** Resources. **Ralf Wagner:** Formal analysis. **Duško Lainšček:** Methodology, Investigation, Formal analysis. **Roman Jerala:** Writing – review & editing, Supervision, Formal analysis, Conceptualization.

Declaration of competing interest

RJ, HE, DL, KM and ŠM are contributors to the patent application describing the invention in this paper.

Data availability

Data will be made available on request.

Appendix A. Supplementary data

Supplementary data to this article can be found online at https://doi.org/10.1016/j.jconrel.2024.05.041.

References

[1] H. Yarlagadda, et al., COVID-19 vaccine challenges in developing and developed countries, Cureus 14 (4) (2022), https://doi.org/10.7759/CUREUS.23951.
[2] S. Mitragotri, Immunization without needles, Nat. Rev. Immunol. 5 (12) (2005) 905–916, https://doi.org/10.1038/nri1728.
[3] A. Flemming, 'Prime and spike' induces mucosal immunity and reduces SARS-CoV-2 transmission, Nat. Rev. Immunol. 22 (12) (2022) 718, https://doi.org/10.1038/s41577-022-00804-2.
[4] M.W. Russell, J. Mestecky, Mucosal immunity: the missing link in comprehending SARS-CoV-2 infection and transmission, Front. Immunol. 13 (2022), https://doi.org/10.3389/FIMMU.2022.957107.
[5] E.C. Lavelle, R.W. Ward, Mucosal vaccines — fortifying the frontiers, Nat. Rev. Immunol. 22 (4) (2021) 236–250, https://doi.org/10.1038/s41577-021-00583-2.
[6] M. Nizard, et al., Mucosal vaccines: novel strategies and applications for the control of pathogens and tumors at mucosal sites, Hum. Vaccin. Immunother. 10 (8) (2014) 2175, https://doi.org/10.4161/HV.29269.
[7] Y. Song, F. Mehl, S.L. Zeichner, Vaccine Strategies to Elicit Mucosal Immunity, 2024, https://doi.org/10.3390/vaccines12020191.
[8] A. Alu, L. Chen, H. Lei, Y. Wei, X. Tian, X. Wei, Intranasal COVID-19 vaccines: from bench to bed, EBioMedicine 76 (2022) 103841, https://doi.org/10.1016/J.EBIOM.2022.103841.
[9] S. Chari, K. Sridhar, C. Kleinstreuer, Effects of subject-variability on nasally inhaled drug deposition, uptake, and clearance, J. Aerosol Sci. 165 (2022) 106021, https://doi.org/10.1016/J.JAEROSCI.2022.106021.
[10] M.E. Armstrong, E.C. Lavelle, C.E. Loscher, M.A. Lynch, K.H.G. Mills, Proinflammatory responses in the murine brain after intranasal delivery of cholera toxin: implications for the use of AB toxins as adjuvants in intranasal vaccines, J. Infect. Dis. 192 (9) (2005) 1628–1633, https://doi.org/10.1086/491739/2/192-9-1628-FIG 002.GIF.
[11] A. Hoffman, D. Stepensky, E. Lavy, S. Eyal, E. Klausner, M. Friedman, Pharmacokinetic and pharmacodynamic aspects of gastroretentive dosage forms, Int. J. Pharm. 277 (1–2) (2004) 141–153, https://doi.org/10.1016/J.IJPHARM.2003.09.047.
[12] Bunavail Buccal: Uses, Side Effects, Interactions, Pictures, Warnings & Dosing - WebMD.. https://www.webmd.com/drugs/2/drug-166704/bunavail-buccal/details (accessed 31 July 2023).
[13] M.S. El-Samaligy, N.N. Afifi, E.A. Mahmoud, Evaluation of hybrid liposomes-encapsulated silymarin regarding physical stability and in vivo performance, Int. J. Pharm. 319 (1–2) (2006) 121–129, https://doi.org/10.1016/J.IJPHARM.2006.04.023.
[14] T.Z. Yang, X.T. Wang, X.Y. Yan, Q. Zhang, Phospholipid deformable vesicles for buccal delivery of insulin, Chem. Pharm. Bull. (Tokyo) 50 (6) (2002) 749–753, https://doi.org/10.1248/CPB.50.749.
[15] C. Karavasili, G.K. Eleftheriadis, C. Gioumouxouzis, E.G. Andriotis, D.G. Fatouros, Mucosal drug delivery and 3D printing technologies: A focus on special patient populations, Adv. Drug. Deliv. Rev. 176 (2021) 113858, https://doi.org/10.1016/J.ADDR.2021.113858.
[16] Z. Zhu, et al., Blue-ringed octopus-inspired microneedle patch for robust tissue surface adhesion and active injection drug delivery, Sci. Adv. 9 (25) (2023), https://doi.org/10.1126/sciadv.adh2213.
[17] S. Hu, et al., A mussel-inspired film for adhesion to wet buccal tissue and efficient buccal drug delivery, Nature Communications 12 (1) (2021) 1–17, https://doi.org/10.1038/s41467-021-21989-5.
[18] V.V. Nair, P. Cabrera, C. Ramírez-Lecaros, M.O. Jara, D.J. Brayden, J.O. Morales, Buccal delivery of small molecules and biologics: of mucoadhesive polymers, films, and nanoparticles - an update, Int. J. Pharm. 636 (2023), https://doi.org/10.1016/J.IJPHARM.2023.122789.
[19] S. Hua, Advances in nanoparticulate drug delivery approaches for sublingual and buccal administration, Front. Pharmacol. 10 (2019), https://doi.org/10.3389/FPHAR.2019.01328.
[20] A. Sette, S. Crotty, Adaptive immunity to SARS-CoV-2 and COVID-19, Cell 184 (4) (2021) 861–880, https://doi.org/10.1016/J.CELL.2021.01.007.
[21] K. Takahashi, et al., Duration of infectious virus shedding by SARS-CoV-2 omicron variant–infected vaccinees, Emerg. Infect. Dis. 28 (5) (2022) 998, https://doi.org/10.3201/EID2805.220197.
[22] S. Sheikh-Mohamed, et al., Systemic and mucosal IgA responses are variably induced in response to SARS-CoV-2 mRNA vaccination and are associated with protection against subsequent infection, Mucosal Immunol. 15 (5) (2022) 799–808, https://doi.org/10.1038/s41385-022-00511-0.
[23] N.J. Mantis, S.J. Forbes, Secretory IgA: arresting microbial pathogens at epithelial Borders, Immunol. Investig. 39 (2010) 383, https://doi.org/10.3109/08820131003622635.
[24] D. Lapuente, et al., Protective mucosal immunity against SARS-CoV-2 after heterologous systemic prime-mucosal boost immunization, Nat. Commun. 12 (1) (2021), https://doi.org/10.1038/S41467-021-27063-4.
[25] C. Agrati, et al., Strong immunogenicity of heterologous prime-boost immunizations with the experimental vaccine GRAd-COV2 and BNT162b2 or ChAdOx1-nCOV19, NPJ Vaccines 6 (1) (2021) 1–4, https://doi.org/10.1038/s41541-021-00394-5.
[26] Y. Tian, J.C. Visser, J.S. Klever, H.J. Woerdenbag, H.W. Frijlink, W.L.J. Hinrichs, Orodispersible films based on blends of trehalose and pullulan for protein delivery, Eur. J. Pharm. Biopharm. 133 (2018) 104–111, https://doi.org/10.1016/J.EJPB.2018.09.016.
[27] A.C. Williams, B.W. Barry, Skin absorption enhancers, Crit. Rev. Ther. Drug Carrier Syst. 9 (3–4) (1992) 305–353.
[28] S. Salehi, S. Boddohi, New formulation and approach for mucoadhesive buccal film of rizatriptan benzoate, Prog. Biomater. 6 (4) (2017) 175, https://doi.org/10.1007/S40204-017-0077-7.
[29] Y. Tian, et al., Development of an Orodispersible Film Containing Stabilized Influenza Vaccine, Pharmaceutics 12 (3) (2020), https://doi.org/10.3390/PHARMACEUTICS12030245.
[30] V. Sugumar, M. Hayyan, P. Madhavan, W.F. Wong, C.Y. Looi, Current development of chemical penetration enhancers for transdermal insulin delivery, Biomedicines 11 (3) (2023) 664, https://doi.org/10.3390/BIOMEDICINES11030664.
[31] A.C. Williams, B.W. Barry, Penetration enhancers, Adv. Drug Deliv. Rev. 56 (5) (2004) 603–618, https://doi.org/10.1016/j.addr.2003.10.025.
[32] B. Grilc, O. Planinšek, Evaluation of monolayer and bilayer buccal films containing metoclopramide, Pharmaceutics 16 (3) (2024) 354, https://doi.org/10.3390/PHARMACEUTICS16030354.
[33] I. Jordan, D. Horn, K. John, V. Sandig, A genotype of modified vaccinia Ankara (MVA) that facilitates replication in suspension cultures in chemically defined medium, Viruses 5 (1) (2013) 321, https://doi.org/10.3390/V5010321.
[34] I. Jordan, D. Horn, K. Thiele, L. Haag, K. Fiddeke, V. Sandig, A deleted deletion site in a new vector strain and exceptional genomic stability of plaque-purified modified vaccinia Ankara (MVA), Virol. Sin. 35 (2) (2020) 212, https://doi.org/10.1007/S12250-019-00176-3.
[35] Z. Ruzsics, F. Lemnitzer, C. Thirion, Engineering adenovirus genome by bacterial artificial chromosome (BAC) technology, Methods Mol. Biol. 1089 (2014) 143–158, https://doi.org/10.1007/978-1-62703-679-5_11.
[36] H. den Braanker, M. Bongenaar, E. Lubberts, How to prepare spectral flow cytometry datasets for high dimensional data analysis: a practical workflow, Front. Immunol. 12 (2021) 768113, https://doi.org/10.3389/FIMMU.2021.768113/BIBTEX.

[37] J.C. Visser, L. Wibier, M. Mekhaeil, H.J. Woerdenbag, K. Taxis, Orodispersible films as a personalized dosage form for nursing home residents, an exploratory study, Int. J. Clin. Pharm. 42 (2) (2020) 436, https://doi.org/10.1007/S11096-020-00990-W.
[38] J.O. Morales, J.T. McConville, Manufacture and characterization of mucoadhesive buccal films, Eur. J. Pharm. Biopharm. 77 (2) (2011) 187–199, https://doi.org/10.1016/J.EJPB.2010.11.023.
[39] A.A. Kassem, D.A.E. Issa, G.S. Kotry, R.M. Farid, Thiolated alginate-based multiple layer mucoadhesive films of metformin forintra-pocket local delivery: in vitro characterization and clinical assessment, Drug Dev. Ind. Pharm. 43 (1) (2017) 120–131, https://doi.org/10.1080/03639045.2016.1224895.
[40] P. Rana, R.S.R. Murthy, Formulation and evaluation of mucoadhesive buccal films impregnated with carvedilol nanosuspension: a potential approach for delivery of drugs having high first-pass metabolism 20 (5) (2013) 224–235, https://doi.org/10.3109/10717544.2013.779331.
[41] J. Mašek, et al., Multi-layered nanofibrous mucoadhesive films for buccal and sublingual administration of drug-delivery and vaccination nanoparticles - important step towards effective mucosal vaccines, J. Control. Release 249 (2017) 183–195, https://doi.org/10.1016/J.JCONREL.2016.07.036.
[42] J.F. Alopaeus, et al., Mucoadhesive buccal films based on a graft co-polymer – a mucin-retentive hydrogel scaffold, Eur. J. Pharm. Sci. 142 (2020) 105142, https://doi.org/10.1016/J.EJPS.2019.105142.
[43] B. Satishbabu, B. Srinivasan, Preparation and evaluation of buccoadhesive films of atenolol, Indian J. Pharm. Sci. 70 (2) (2008) 175, https://doi.org/10.4103/0250-474X.41451.
[44] B. Grilc, J. Zdovc, O. Planinšek, Advanced flow cell design for in vitro release testing of mucoadhesive buccal films, Acta Pharmaceutica 70 (3) (2020) 359–371, https://doi.org/10.2478/ACPH-2020-0030.
[45] T. Ura, K. Okuda, M. Shimada, Developments in viral vector-based vaccines, Vaccines (Basel) 2 (3) (2014) 624–641, https://doi.org/10.3390/VACCINES2030624.
[46] J.T. Bulcha, Y. Wang, H. Ma, P.W.L. Tai, G. Gao, Viral vector platforms within the gene therapy landscape, Signal Transd. Target. Ther. 6 (1) (2021) 1–24, https://doi.org/10.1038/s41392-021-00487-6.
[47] S.A. Mendonça, R. Lorincz, P. Boucher, D.T. Curiel, Adenoviral vector vaccine platforms in the SARS-CoV-2 pandemic, NPJ Vaccines 6 (1) (2021) 1–14, https://doi.org/10.1038/s41541-021-00356-x.
[48] I. Bajrovic, S.C. Schafer, D.K. Romanovicz, M.A. Croyle, Novel technology for storage and distribution of live vaccines and other biological medicines at ambient temperature, Sci. Adv. 6 (10) (2020) 4819, https://doi.org/10.1126/sciadv.aau4819.
[49] A. Volz, G. Sutter, Modified vaccinia virus Ankara: history, value in basic research, and current perspectives for vaccine development, Adv. Virus Res. 97 (2017) 187–243, https://doi.org/10.1016/BS.AIVIR.2016.07.001.
[50] Z. Ghaemmaghamian, R. Zarghami, G. Walker, E. O'Reilly, A. Ziaee, Stabilizing vaccines via drying: quality by design considerations, Adv. Drug Deliv. Rev. 187 (2022) 114313, https://doi.org/10.1016/J.ADDR.2022.114313.
[51] M.D. Cain, et al., Virus entry and replication in the brain precedes blood-brain barrier disruption during intranasal alphavirus infection, J. Neuroimmunol. 308 (2017) 118, https://doi.org/10.1016/J.JNEUROIM.2017.04.008.
[52] L.A. Bors, F. Erdö, Overcoming the blood–brain barrier. Challenges and tricks for CNS drug delivery, Sci. Pharm. 87 (1) (2019) 6, https://doi.org/10.3390/SCIPHARM87010006.
[53] I. Abdalrhman, I. Gurt, E. Katz, Protection induced in mice against a lethal orthopox virus by the lister strain of vaccinia virus and modified vaccinia virus Ankara (MVA), Vaccine 24 (19) (2006) 4152–4160, https://doi.org/10.1016/J.VACCINE.2006.02.012.
[54] O.V. Orlova, D.V. Glazkova, E.V. Bogoslovskaya, G.A. Shipulin, S.M. Yudin, Development of modified vaccinia virus Ankara-based vaccines: advantages and applications, Vaccines (Basel) 10 (9) (2022), https://doi.org/10.3390/VACCINES10091516.
[55] D. Lainšček, et al., A Nanoscaffolded spike-RBD vaccine provides protection against SARS-CoV-2 with minimal anti-scaffold response, Vaccines (Basel) 9 (5) (2021), https://doi.org/10.3390/VACCINES9050431.
[56] A. Thess, et al., Sequence-engineered mRNA without chemical nucleoside modifications enables an effective protein therapy in large animals, Mol. Ther. 23 (9) (2015) 1456–1464, https://doi.org/10.1038/MT.2015.103.
[57] A.M. Reichmuth, M.A. Oberli, A. Jeklenec, R. Langer, D. Blankschtein, mRNA vaccine delivery using lipid nanoparticles, Ther. Deliv. 7 (5) (2016) 319–334, https://doi.org/10.4155/TDE-2016-0006.
[58] E. Blanco, H. Shen, M. Ferrari, Principles of nanoparticle design for overcoming biological barriers to drug delivery, Nat. Biotechnol. 33 (9) (2015) 941–951, https://doi.org/10.1038/NBT.3330.
[59] P.R. Cullis, M.J. Hope, Lipid nanoparticle systems for enabling gene therapies, Mol. Ther. 25 (7) (2017) 1467–1475, https://doi.org/10.1016/J.YMTHE.2017.03.013.
[60] H.H. Tam, et al., Sustained antigen availability during germinal center initiation enhances antibody responses to vaccination, Proc. Natl. Acad. Sci. USA 113 (43) (2016) 6639–6648, https://doi.org/10.1073/PNAS.1606050113.
[61] T. Mao, et al., Unadjuvanted intranasal spike vaccine elicits protective mucosal immunity against sarbecoviruses, Science 378 (6622) (2022), https://doi.org/10.1126/science.abo2523.
[62] E.J. Wherry, D.H. Barouch, T cell immunity to COVID-19 vaccines, Science (1979) 377 (6608) (2022) 821–822, https://doi.org/10.1126/SCIENCE.ADD2897.
[63] C. Zhong, et al., Mucosal vaccination induces protection against SARS-CoV-2 in the absence of detectable neutralizing antibodies, NPJ Vaccines 6 (1) (2021) 1–7, https://doi.org/10.1038/s41541-021-00405-5.
[64] M.Y. Zanna, et al., Review of dendritic cells, their role in clinical immunology, and distribution in various animal species, Int. J. Mol. Sci. 22 (15) (2021), https://doi.org/10.3390/IJMS22158044.
[65] N. Pakpour, C. Zaph, P. Scott, The central memory CD4+ T cell population generated during Leishmania major infection requires IL-12 to produce IFN-γ, J. Immunol. 180 (12) (2008) 8299, https://doi.org/10.4049/JIMMUNOL.180.12.8299.
[66] M. Spadaro, M. Caldano, F. Marnetto, A. Lugaresi, A. Bertolotto, Natalizumab treatment reduces L-selectin (CD62L) in CD4+ T cells, J. Neuroinflammation 12 (1) (2015) 1–9, https://doi.org/10.1186/S12974-015-0365-X/FIGURES/4.
[67] H. Guan, P.S. Nagarkatti, M. Nagarkatti, Role of CD44 in the Differentiation of Th1 and Th2 Cells: CD44-Deficiency Enhances the Development of Th2 Effectors in Response to Sheep RBC and Chicken Ovalbumin, The J. Immunology 183 (1) (2009) 172–180, https://doi.org/10.4049/JIMMUNOL.0802325.
[68] L.K. Beura, et al., CD4+ resident memory T cells dominate immunosurveillance and orchestrate local recall responses, J. Exp. Med. 216 (5) (2019) 1214, https://doi.org/10.1084/JEM.20181365.
[69] J. Tang, et al., Respiratory mucosal immunity against SARS-CoV-2 after mRNA vaccination, Sci. Immunol. 7 (76) (2022) 4853, https://doi.org/10.1126/sciimmunol.add48.
[70] S. Aminu, M.A. Ibrahim, A.B. Sallau, Interaction of SARS-CoV-2 spike protein with angiotensin converting enzyme inhibitors and selected compounds from the chemical entities of biological interest, Beni Suef. Univ. J. Basic Appl. Sci. 10 (1) (2021), https://doi.org/10.1186/S43088-021-00138-3.
[71] R.C. Mettelman, E.K. Allen, P.G. Thomas, Mucosal immune responses to infection and vaccination in the respiratory tract, Immunity 55 (5) (2022) 749, https://doi.org/10.1016/J.IMMUNI.2022.04.013.
[72] A.V. Wisnewski, J.C. Luna, C.A. Redlich, Human IgG and IgA responses to COVID-19 mRNA vaccines, PLoS ONE 16 (6) (2021), https://doi.org/10.1371/JOURNAL.PONE.0249499.
[73] I. Quinti, E.P. Mortari, A. Fernandez Salinas, C. Milito, R. Carsetti, IgA antibodies and IgA deficiency in SARS-CoV-2 infection, Front. Cell. Infect. Microbiol. 11 (2021), https://doi.org/10.3389/FCIMB.2021.655896.
[74] Y. Takamatsu, et al., SARS-CoV-2-neutralizing humoral IgA response occurs earlier but is modest and diminishes faster than IgG response, Microbiol. Spectr. 10 (6) (2022), https://doi.org/10.1128/spectrum.02716-22.
[75] E. Tchilian Sewell, et al., Pigs systemic antibody immune responses in induces powerful protective local T cell and immunization with influenza vaccine simultaneous aerosol and intramuscular, J. Immunol. (2021), https://doi.org/10.4049/jimmunol.2001086.
[76] M.A. Kutzler, D.B. Weiner, DNA vaccines: ready for prime time? Nat. Rev. Genet. 9 (10) (2008) 776–788, https://doi.org/10.1038/nrg2432.
[77] S. Manoj, L.A. Babiuk, S. Van Drunen Littel-van, Den Hurk, Approaches to enhance the efficacy of DNA vaccines, Crit. Rev. Clin. Lab. Sci. 41 (1) (2004) 1–39, https://doi.org/10.1080/10408360490269251.
[78] S. Velmurugan, S. Dodla, Buccal penetration enhancers-an overview, Asian J. Pharm. Clin. Res. 6 (3) (2013) 39–47.
[79] V.V. Prasanth, A. Puratchikody, S.T. Mathew, K.B. Ashok, Effect of permeation enhancers in the mucoadhesive buccal patches of salbutamol sulphate for unidirectional buccal drug delivery, Res. Pharm. Sci. 9 (4) (2014) 259–268.
[80] B. KumarV, et al., Formulation design, in vitro evaluation and stability studies on mucoadhesive buccal films of anti-anginal calcium channel blocker, J. Appl. Pharm. Sci. 06 (2011) 136–142.
[81] C. Dawes, Estimates, from salivary analyses, of the turnover time of the oral mucosal epithelium in humans and the number of bacteria in an edentulous mouth, Arch. Oral Biol. 48 (5) (2003) 329–336, https://doi.org/10.1016/S0003-9969(03)00014-1.
[82] M. Kouchak, S. Handali, Effects of various penetration enhancers on penetration of aminophylline through shed Snake skin, Jundishapur J. Nat. Pharm. Prod. 9 (1) (2014) 24, https://doi.org/10.17795/JJNPP-12904.
[83] N. Hassan, A. Ahad, M. Ali, J. Ali, Chemical permeation enhancers for transbuccal drug delivery, Expert Opin. Drug Deliv. 7 (1) (2010) 97–112, https://doi.org/10.1517/17425240903338758.
[84] I. Som, K. Bhatia, M. Yasir, Status of surfactants as penetration enhancers in transdermal drug delivery, J. Pharm. Bioallied Sci. 4 (1) (2012) 2, https://doi.org/10.4103/0975-7406.92724.
[85] R. Shimosakai, I.A. Khalil, S. Kimura, H. Harashima, mRNA-loaded lipid nanoparticles targeting immune cells in the spleen for use as Cancer vaccines, Pharmaceuticals 15 (8) (2022), https://doi.org/10.3390/PH15081017/S1.
[86] T. Travieso, J. Li, S. Mahesh, J.D.F.R.E. Mello, M. Blasi, The use of viral vectors in vaccine development, NPJ Vaccines 7 (1) (2022) 1–10, https://doi.org/10.1038/s41541-022-00503-y.
[87] M. Cokarić Brdovčak, et al., ChAdOx1-S adenoviral vector vaccine applied intranasally elicits superior mucosal immunity compared to the intramuscular route of vaccination, Eur. J. Immunol. 52 (6) (2022) 936–945, https://doi.org/10.1002/EJI.202249823.
[88] A. Popov, Mucus-penetrating particles and the role of ocular mucus as a barrier to micro- and nanosuspensions, J. Ocul. Pharmacol. Ther. 36 (6) (2020) 366, https://doi.org/10.1089/JOP.2020.0022.
[89] N. Elahpour, F. Pahlevanzadeh, M. Kharaziha, H.R. Bakhsheshi-Rad, S. Ramakrishna, F. Berto, 3D printed microneedles for transdermal drug delivery: a brief review of two decades, Int. J. Pharm. 597 (2021), https://doi.org/10.1016/J.IJPHARM.2021.120301.